TAMPERE UNIVERSITY OF TECHNOLOGY

ELENA RUEDA ROMERO
FINITE ELEMENT SIMULATION OF A BOLTED STEEL JOINT IN FIRE USING ABAQUS PROGRAM
Master of Science Thesis

ABSTRACT

The research on the performance of steel connections at elevated temperatures is of great importance for the understanding of structural collapses caused by fire; concerning fire safety in building design. The joints of any steel building are significant structural components, as they provide links between principal members. This study presents a detailed three-dimensional (3-D) finite element (FE) model of a steel endplate beam-to-column joint subjected to simulations at ambient and elevated temperatures. The model was defined using ABAQUS software, on the basis of experimental tests performed in Al-Jabri *et al.*, 1999. Good agreement between simulations and experimental observations confirms that the finite element ABAQUS solver is suitable for predicting the behaviour of the structural steel joint in fire. Using the European standards (EN 1993-1-8, 2005), a component based model was also developed to predict the behaviour of the joint, and to compare against the FE model at both ambient and elevated temperatures. Comparison of the results provided a high level of accuracy between models, especially in the elastic zone.

The validated FE model was used to conduct further studies with new 3D loading conditions in order to enhance the understanding of steel joints behaviour on fire. The Component Method model was extended and compared against ABAQUS model, providing useful results which enforced the use of this method on 3D.

PREFACE

This study was realized at Tampere University of Technology, Department of Structural Engineering, in the Research Centre of Metal Structures. The study was guided and supervised by Professor Markku Heinisuo.

I would first like to express my deepest gratitude to Professor Markku Heinisuo for giving me the opportunity to work in the Department of Structural Engineering, and for all the guidance and supervision given to my work. I would also like to thank to the Centre of Metal Structures for letting me participate in the department and for contribute in the widening of my knowledge on metal structures field. My grateful thanks are also due to Reijo Lindgren for helping me with ABAQUS, especially at the beginning of this study. My warmest acknowledgements are due to Hilkka Ronni for her kind assistance and help during the time I have been working in the department. I would also like to thank my workmates for a pleasant environment and for being interpreters of Finnish language for me in many occasions.

I would like to express my sincere gratitude to Lucía, Quique, Debbie and Vero for being my family in Finland. My life in Tampere would have never been the same without you. I am very grateful to all my friends from Tampere for their support, help and friendship; and for sharing with me the amazing experience of living in Finland as exchange students.

I owe my most sincere gratitude to my family and friends for their encouragement and love during my life; especially to my parents Maria Antonia and Jose Antonio, and my sister Paloma. The last but not the least, I would like to thank my boyfriend Gaby for his support during this year. I really appreciate your unfailing patience and love despite of being separated for so long.

Tampere, July 2010.

ELENA RUEDA ROMERO

TABLE OF COTENTS

NOMENCLATURE

Δl	Elongation
α	Thermal expansion coefficient
α_1, α_2	Yielding line factor
γ_{M0}	Partial safety factor of resistance of cross sections
γ_{M2}	Partial safety factor for resistance of cross-sections in tension to fracture
ε_θ	Relative thermal elongation
ε_p	Strain at the proportional limit
ε_{pl}	Plastic strain
ε_t	Yield strain
ε_u	Ultimate strain
ε_y	Limiting strain for yield strength
θ_a	Temperature
η	Stiffness ratio
λ_p	Endplate slenderness
μ	Friction coefficient
ρ	Reduction factor for plate buckling
σ	Stress
υ	Poisson's ratio
φ	Rotation
ω	Reduction factor for interaction with shear
A_s	Tensile stress area
A_v	Shear area
D_{km}	Mean screw diameter
E	Young's modulus
$F_{c,Rd}$	Design compression resistance
F_M	Bolt pretension load
$F_{t,Rd}$	Design tension resistance
L_b	Bolt elongation

M	Bending moment
M_A	Bolt installation torque
$M_{c,Rd}$	Design moment resistance for bending
$M_{j,Rd}$	Design moment resistance
$M_{pl,Rd}$	Plastic moment resistance
P	Bolt pintch
S_j	Rotational stiffness
V	Shear force
V_{Rd}	Design shear resistance
W_{pl}	Pastic section modulus
a	Weld thickness
b_{eff}	Effective width
b_f	Width of flange
b_p	Width of endplate
d	Clear depth
e	Horizontal distance from bolt to edge of endplate or column flange
f_p	Proportional limit
f_u	Ultimate tensile strength
f_y	Yield strength
h_b	Height of beam
h_r	Distance from bolt row to the centre of compression
$k_{b,\theta}$	Reduction factor for bolts
$k_{E,\theta}$	Reduction factor for Young's modulus
$k_{f,\theta}$	Reduction factor for yield strength
k_i	Stiffness coefficient
$k_{p,\theta}$	Reduction factor for proportional limit
l	Length of steel
l_{eff}	Effective length
$l_{eff,cp}$	Effective length for circular patterns
$l_{eff,np}$	Effective length for noncircular patterns

m	Horizontal distance from bolt to column or beam web
p	Distance between bolt rows
p_h	Horizontal spacing between bolt holes
r	Radius
t_{bh}	Thickness of bolt head
t_{bn}	Thickness of bolt nut
t_f	Thickness of flange
t_p	Thickness of endplate
t_w	Thickness of web
u	Displacement
z	Lever arm

1.   INTRODUCTION

1.1.   Background

Steel structures have always had the advantages of lightness, stiffness and strength, as well as rapid construction when compared with other construction materials. However, at elevated temperatures steel behavior is seriously affected with the lost of both strength and stiffness, leading to large deformations and often collapse of the structures. The overall design of steel structures is directly linked to the design of their joints, since they provide interaction between the other principal structural components and contribute to the overall building stability. When fire conditions occur, the joints have a considerable effect on the survival time of the structure due to their ability to redistribute forces. As a result, joints can be considered the critical part of the design of steel structures, and the investigation of their behaviour remains one of the main subjects for fire engineering research.

Understanding about the behaviour of joints is enhanced by developing analytical models. Various forms of analysis and mathematical modelling methods have been suggested in order to study the semi-rigid characteristics of beam-to-column joints and their influence on the response of the rest of the structural members. The European standards for the design of steel structures (EN 1993-1-8, 2005) include a simplified analytical model to analyze structural steel joints at ambient temperature, known as the Component Method. This method determines the behaviour of a steel joint by assembling the individual behaviour for each active component into a spring model. Wang, *et al*., 2006; Hu, *et al*., 2009 and Al-Jabri, *et al*., 2005 developed component based models for simulating endplate joints between beams and columns in steel framed structures in fire conditions. The variation on the material properties of structural steel on fire was used in order to represent the elevated temperatures in the models. On the Component Method, each component has its own temperature-dependent load-displacement curve, and the whole joint therefore interact realistically with the surrounding structure.

Experimental investigations have also been conducted on the performance of steel joints at elevated temperatures. Al-Jabri *et al*., 1999 performed experimental tests to typical steel beam-to-column joints which made possible the establishment of full moment-rotation-temperature characteristics. Although laboratory fire tests provide acceptable results, in many cases experiments are either not feasible or too expensive to perform. Nowadays it is possible to simulate complex real world cases where a wide range of

parameters are difficult to treat in the laboratory, using numerical modelling methods. Finite Element Method (FEM) has become a satisfactory tool giving predictions of the response of steel joints next to failure deformations (Sarraj, 2007; Yu, 2008).

1.2. Goal of Study

For the study of this thesis an endplate beam-to-column joint configuration was simulated with a detailed 3D Finite Element model. The simulation was carried out at both ambient and elevated temperatures, by employing ABAQUS software. The model counts with a great complexity since it has material nonlinearity, large deformation and contact behaviour. European standards (EN 1993-1-1-2, 2005) were used to define the material properties of the steel at elevated temperatures for components and bolts used in the model.

Applying the Component Method to the endplate joint according to EN 1993-1-1, 2005 and EN 1993-1-8, 2005, it was possible to give a prediction about the joint behaviour which was used to compare against the Finite Element model at both ambient and fire temperatures. The model has also been evaluated against available experimental data at elevated temperatures (Al-Jabri, 1999).

After determining a satisfactory level of accuracy of the model using the previous comparisons, the study has been extended for analysis with new 3D loading conditions at both ambient and elevated temperatures.

2. BEHAVIOUR OF BEAM-TO-COLUMN JOINTS AT ELEVATED TEMPERATURES

2.1. Introduction to Beam-to-column Joints

The word connection refers to the structural steel components which mechanically fasten the members within the structure. Such components include the bolts, endplate, web and flanges of beams and columns. Traditionally the behaviour between beam and column of steel framed structures is considered either rigid (implying complete rotational continuity) or pinned (implying no moment resistance). In reality both of these characteristics are merely extreme examples. Most pinned joints possess some rotational stiffness while rigid joints display some flexibility. Therefore, it seems reasonable to categorise most joints as semi-rigid. The primary function of a semi-rigid joint is to facilitate transfer of forces and moments between the beams and the supporting columns. The effect of joint rigidity on the transfer of moments on the beam is shown in Figure 2.1.
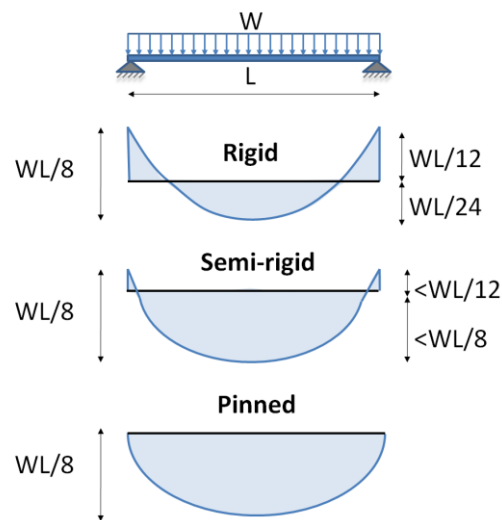
Figure 2.1*: Effect of joint characteristics on beam behaviour.*

A beam-to-column joint is usually subject of bending moments, shearing force, axial force and torsion. The rotational behaviour is the most important of the beam-to-column joints' properties since it can have a significant influence on the structural frame response. The rotational characteristic of a joint is usually represented by a moment-rotation relationship. When loads are applied to the joint, a moment M is induced causing a rotation φ. This rotation is the change in the angle between the end of the beam and the column face as shown Figure 2.2. The effect on the frame behaviour of

the other forces may be assumed to be insignificant since the axial and shearing deformations have only a small influence in comparison with the rotational deformation.
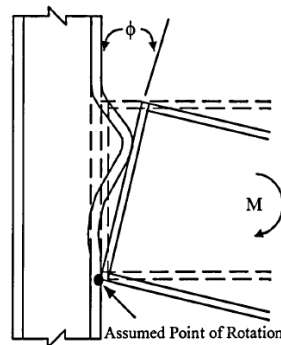
Figure 2.2*: Moment-rotation characteristi.*

Various types of joints exist, and the moment-rotation behaviour varies gradually between extremes cases; from the most flexible joints until rigid joints. Among the different forms of joint commonly used in the construction industry the most popular are endplate and cleat joints. Figure 2.3 shows an example for each of these joint types.
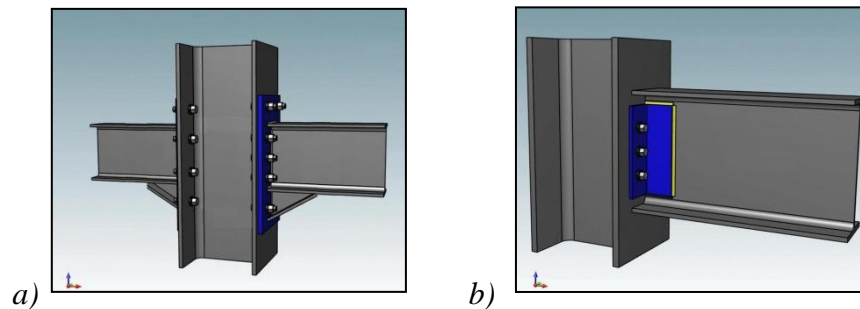
Figure 2.3*: Joint types. a) Endplate, b) Cleat.*

2.2. Material Properties of Structural Steel at Elevated Temperatures

The mechanical properties of all common building materials change with increasing temperatures. When structural steel is exposed to fire it suffers a progressive loss of strength and stiffness due to its high thermal conductivity. This phenomenon may cause possible excessive deformation in structural elements and lead to failure.

To allow an understanding of the behaviour of steel joints exposed to fire, it is necessary to investigate the influence of temperature on the mechanical properties of structural steel. The mechanical properties are described mainly by the stress-strain relationship. This relationship in a standard steel specimen under tension stresses and at ambient temperature is established as illustrates Figure 2.4.
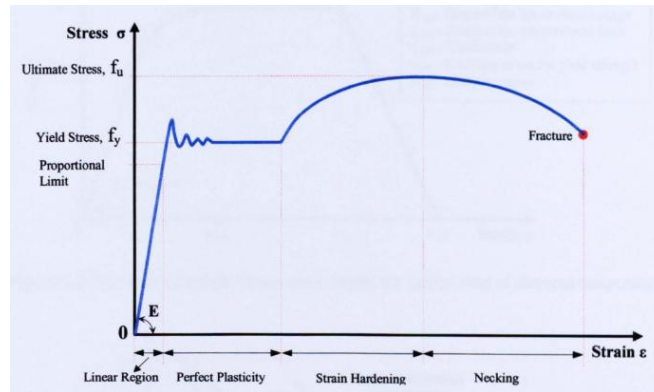
Figure 2.4*: Stress-strain relationship for carbon steel at ambient temperatures.*

The stress-stain relationship for steel at elevated temperatures is usually obtained from experimentation. Two methods exist of determining this characteristic, which difference the results obtained, and so the mechanical properties that can be used for structural steel. The experimental methods are *state* and *transient* tests. On *state tests* the tensile specimen is subject to a constant temperature and load is increased. The stress-strain response is therefore appropriate for a given temperature. Alternatively, in *transient tests* the specimen is subjected to a constant load, and the temperature is increased in a pre-determined rate, with resulting strains being recorded. *Transient tests* result to be more representative of actual stress-strain characteristics in frame behaviour and for Eurocodes they are accepted relating to the resistance of steel structures. This method has been shown to provide reliable results and yield adequate data. Transient stress-stain relationship includes time effect, so no creeping need to be modeled when applying this relationship in analysis. Moreover, they can be said to reflect a closest situation of real building fires.

The Finite Element model developed for this thesis was subjected to simulations of transient tests based on the experiments performed at Al Jabri *et al*., 1999. The model was undergone to a uniform increase of temperature; while constant loading conditions were applied.

2.2.1. Degradation of structural steel at elevated temperatures on Finite Element model

On the Finite Element model of the beam-to-column joint that was carried out for this thesis, elevated temperatures are involved. This means that material properties needed to be carefully defined. For the degradation of steel properties it was considered the stress-strain relationship and the thermal elongation by using Eurocode's recommendations. EN 1993-1-2 describes the stress-strain curve for carbon steel at elevated temperature as shown in Figure 2.5. It is defined by a linear-elliptical curve

where the strain limits are established at 2% for yield strain, 15% for limiting strain for yield strength and 20% as ultimate strain.
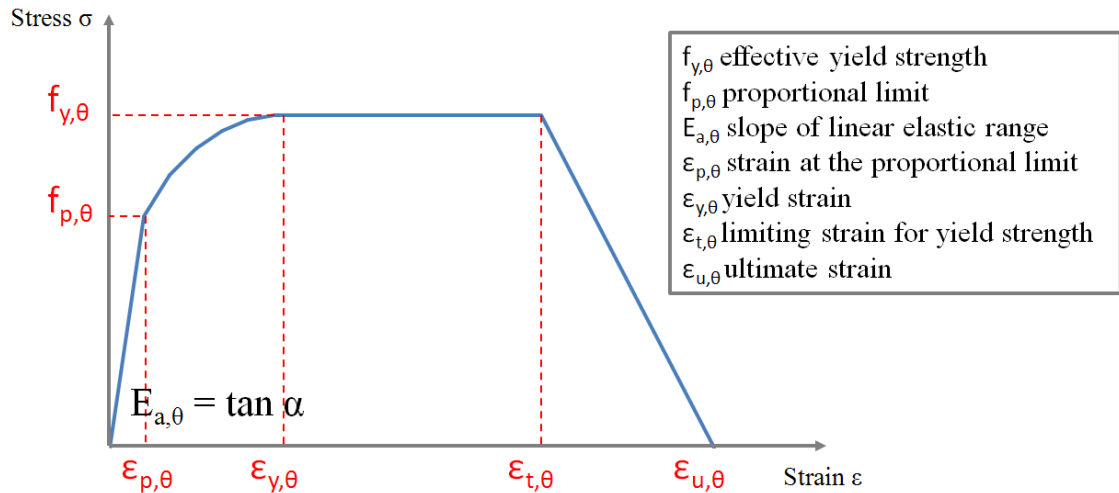
Figure 2.5*: Tri-linear-elliptical Stress-strain model for carbon steel at elevated temperatures.*

In the Finite Element model of the joint studied for this thesis, it was assumed this behavior for the steel used in both components and bolts. In order to describe the degradation of the material properties at elevated temperatures in the stress-strain relationship, reduction factors (Figure 2.6) are introduced for yield strength, proportional limit and the Young's modulus according to standards. Figure 2.7 shows the mechanical behaviour at ambient and elevated temperatures of the steel which was described for the components of the simulated joint. Young's modulus and yield strength established at ambient temperature were 197 GPa, and of 322 MPa, respectively.
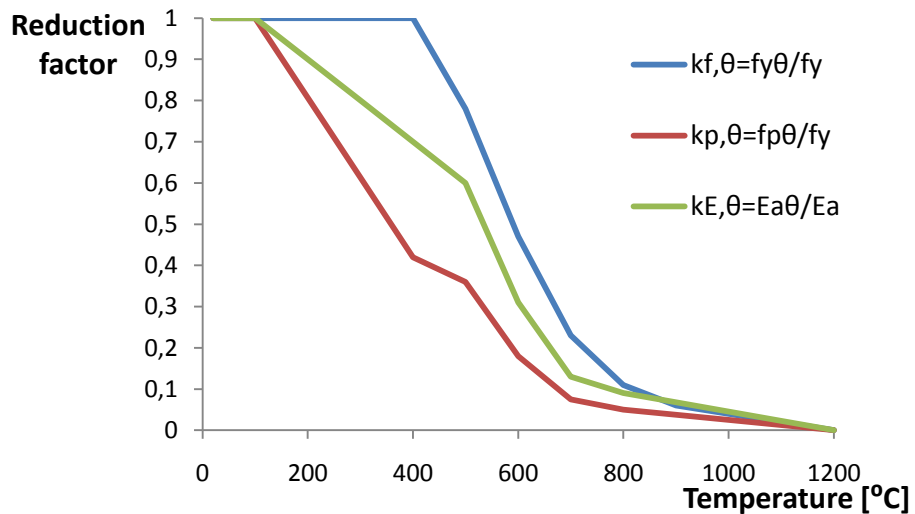
Figure 2.6*: Reduction factors for stress-strain curve of carbon steel at elevated temperatures (EN 1993-1-2, 2005).*
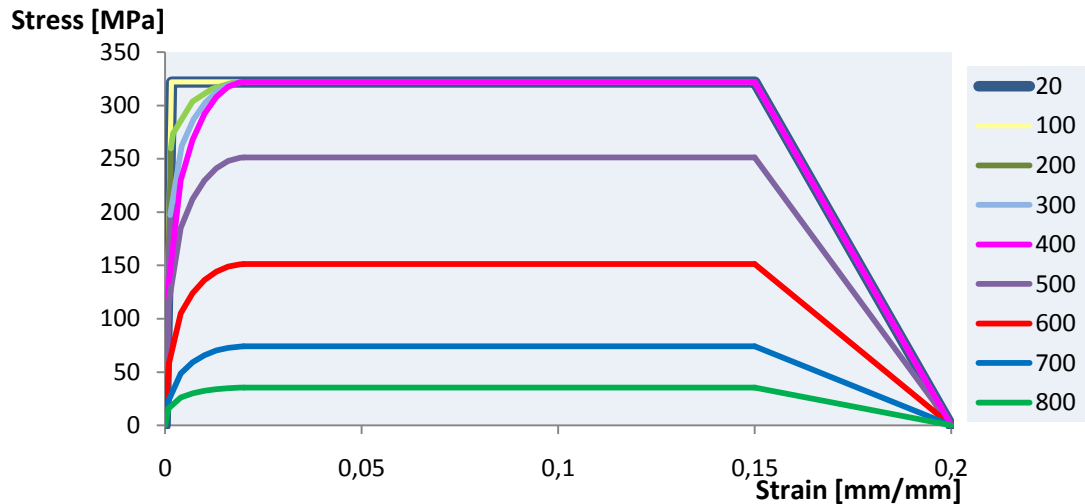
Figure 2.7*: EC3 stress-strain relationship at elevated temperatures for steel Grade 43, with mechanical properties: E = 197 GPa, fy = 322 MPa.*

In FEM analysis the stress-strain modes do not include the decreasing phase. Instead, during the study of the results, steel rupture will be considered 20% from Eurocode, and the effect of the maximum plastic strains allowed (5%, 10%, 15%, 20%) will be shown in the case of study. Moreover, maximum strains of grade 8.8 bolts at ambient and elevated temperatures will be considered based on Theodorou *et al.,* 2001.

It is known that the expansion of steel becomes significant at elevated temperatures. Thermal elongation of steel is determined in conjunction with steel temperature by Eurocode 3 (EN 1993-1-2, 2005). It is defined using expressions 2.1-2.3. Figure 2.8 shows the evolution of elongation as a function of temperature. For the Finite Element model, this configuration of the steel thermal elongation was adopted during the simulations in fire.

for $20ºC < \theta_a < 750ºC$:

$$\Delta l/l = 1{,}2 \times 10^{-5} \theta_a + 0{,}4 \times 10^{-8} \theta_a^2 - 2{,}416 \times 10^{-4} \tag{2.1}$$

for $750ºC < \theta_a < 860ºC$:

$$\Delta l/l = 1{,}1 \times 10^{-2} \tag{2.2}$$

for $860ºC < \theta_a < 1200ºC$:

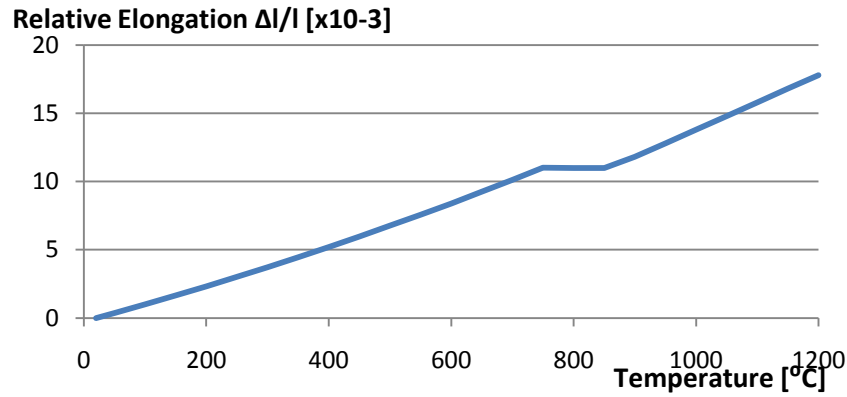$$\Delta l/l = 2 \times 10^{-5} \theta_a - 6{,}2 \times 10^{-3} \tag{2.3}$$

where

l is the length at 20°C,

Δl is the temperature induced elongation,

$\Delta l/l = \varepsilon_\theta$ is the relative thermal elongation,

θ_a is the steel temperature [°C].

Figure 2.8: *Thermal elongation of carbon steel as a function of temperature.*

2.2.2. Degradation of the joint's characteristics at elevated temperatures in Component Method

On the following chapter the Component Method is used for the analysis of the studied joint. As it happens with the Finite Element model the performance of steel properties at elevated temperatures has to be taken into account. In this case the important parameters defining joint properties are the strength and stiffness. The degradation applied for strength and stiffness of the components was based on the degradation of structural steel at elevated temperatures according to EC 1993-1-2, 2005. For the reduction of the rotational stiffness at elevated temperatures it was applied the reduction factors for Young's modulus $k_{E,\theta}$, while for the moment design resistance it was used the reduction factors for bolts $k_{b,\theta}$ or the reduction factor for yield strength $k_{f,\theta}$ (Table 2.1). Factor $k_{b,\theta}$ is meant for bolts and bearing strength in the joints, and factor $k_{f,\theta}$ is for steel parts. In order to see the effect of both reductions, they are used on the Component Method model separately.

Table 2.1: *Properties of structural steel at elevated temperatures.*

Steel temperature (°C)	Reduction factors for Young's modulus $k_{E,\theta}$, bolts $k_{b,\theta}$ and yield strength $k_{f,\theta}$ at temperature θ		
	$k_{E,\theta}$	$k_{b,\theta}$	$k_{f,\theta}$
20	1,000	1,000	1,000
100	1,000	0,968	1,000
200	0,900	0,935	1,000
300	0,800	0,903	1,000
400	0,700	0,775	1,000
500	0,600	0,550	0,780
600	0,310	0,220	0,470
700	0,130	0,100	0,230
800	0,090	0,067	0,110

3.   COMPONENT METHOD

The Eurocodes form a common European set of structural design codes for buildings and other civil engineering works. EN 1993 Eurocode 3 is applied for the design of steel structures, where the basis of design concerns about requirements for resistance, serviceability, durability and fire resistance. EN 1993, Part 1 − 8: Joints, provides detailed rules to determine the structural behaviour of joints in terms of resistance (moment capacity), stiffness (rotational stiffness) and deformation capacity (rotation capacity). The procedures given are based on the Component Method, which determines the structural properties of the joint from the structural behaviour of all relevant components out of which the joint is composed. One component in the analysis model presents one physical component or feature of the joint. The feature can be bolt, weld and end-plate in bending or similar.

The Component Method reproduces the total response of the joint as an assembly of the partial responses of the individual components. In this context, a joint is proposed as a linear string-component system as shows Figure 3.1 a). The result of the combination of the system is a representation of the joint in the form of a rotational stiffness spring connecting the centre of the connected members at the point of intersection (Figure 3.1b).

a) Joint-String system   *b) Model*
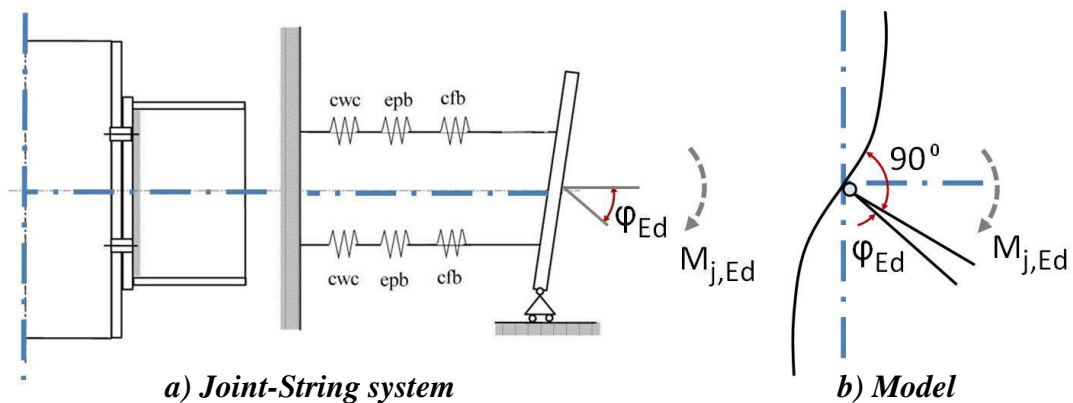
Figure 3.1: *Joint configuration as a rotational stiffness string. The joint properties can be represented as a moment-rotation characteristic*

The method of standard (EN 1993-1-8, 2005) is applied only to planar joints. The method can be used to construct the local analysis models for many kinds of joints such as beam-to-column joints and base bolt joints. The case that concerns this thesis is a beam-to-column double sided joint with bolted endplate joint. The structural properties

of the joint have been determined following Eurocode 3, by the application of the Component Method.

3.1. Terms and Definitions

In the component method a *basic component* is defined as one single part of the joint that contributes to one or more of its structural properties. *Connection* is the location at which two or more elements meet, and for design purposes it is the assembly of the *basic components* required to represent the behavior during the transfer of the relevant internal forces and moments at the joint. Finally, the *joint* is the zone where two or more members are interconnected. For example, a double-sided *joint* configuration consists of a column web panel in shear *component* and two *connections,* as shows Figure 3.2 (EN-1-8 2005).
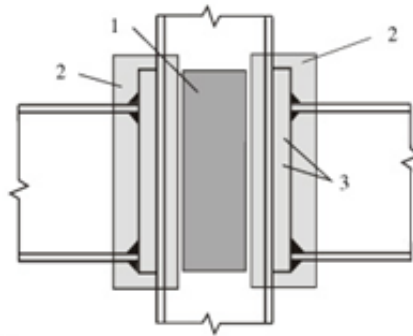
Figure 3.2 *Double-sided joint configuration. 1. web panel in shear, 2.connectiont, 3. components (figure from EN 1993-1-8 2005).*

For extended and flush endplate joints, the component method use T-stub elements to represent the components in the tension zone. This is implemented by adopting appropriate orientation of the idealized T-stub components in order to account for the deformation due to the column flange and the endplate in bending. Three different failure modes can be observed for T-stub components represented on Figure 3.3. The failure modes are total yield of flange (Mode 1), yield of flange and bolts together (Mode 2), and yield of bolts only (Mode 3), (EN 1993-1-8 2005).

a) Mode 1   *b) Mode 2*   *c) Mode 3*
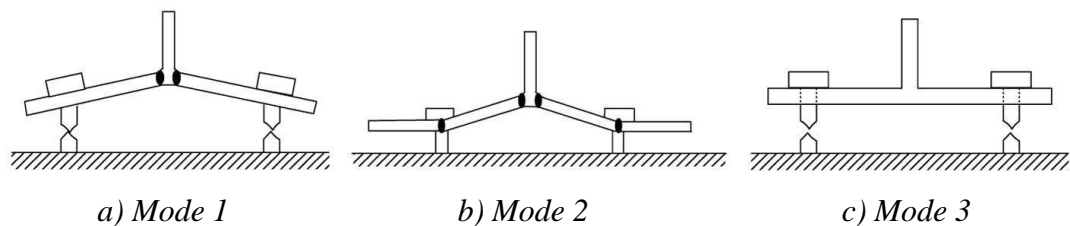
Figure 3.3*: Failure mode of a T-stub.*

3.2. Studied Case

A cruciform bolted beam-to-column steel joint tested experimentally by Al-Jabri at elevated temperatures, was considered in the analysis which accomplishes this thesis. Al-Jabri performed three groups of tests on beam-to-column joints and Group 1 was used for this study. The joint consists of two UB 254x102x22 beams connected to a UC 152x152x23 column using twelve M16 bolts and 8 mm thick endplates. Joint details and the dimensions of all the components are shown in Figure 3.4. For a realistic comparison among calculations obtained from compo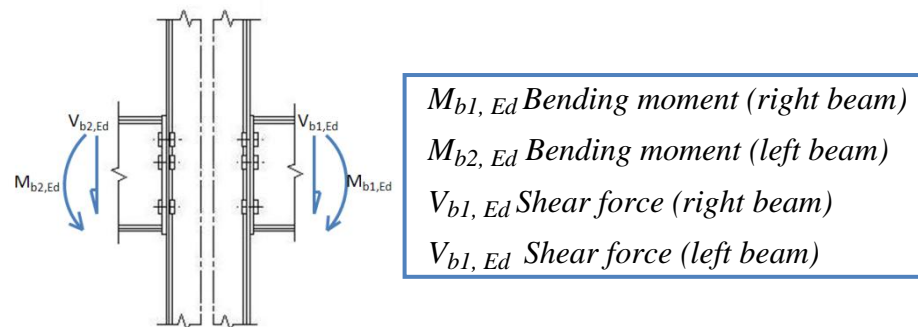nent method, ABAQUS model and test results; this joint configuration is used for all analysis at ambient and elevated temperatures.
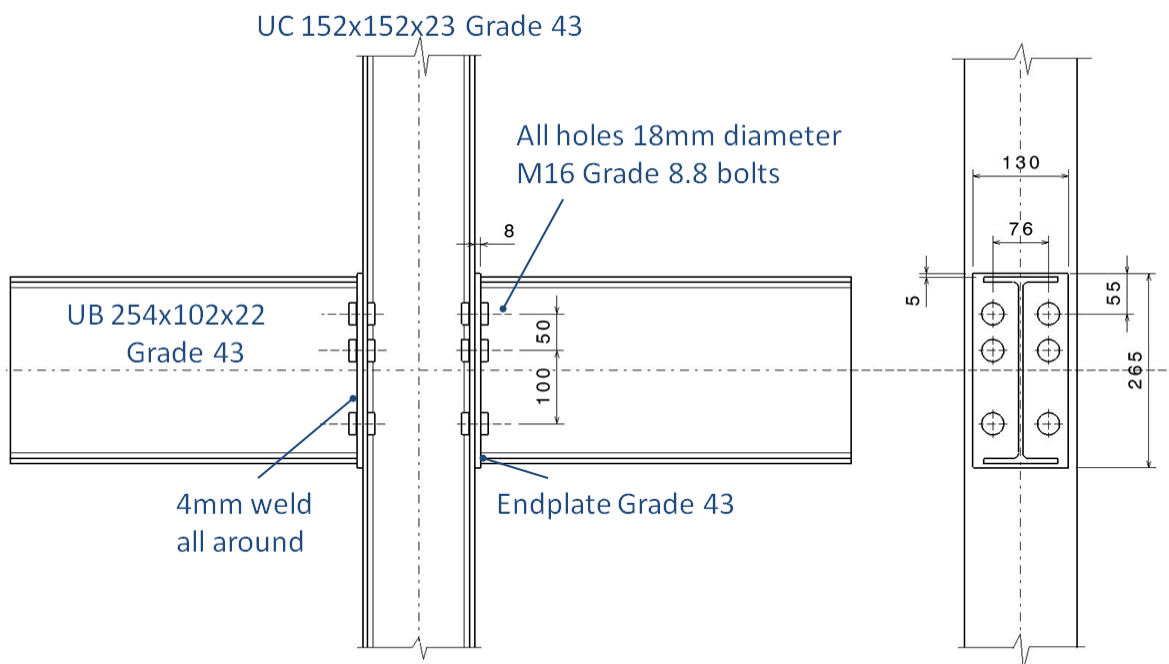
Figure 3.4: Geometry and connection details.

The loading arrangement adopted on Al-Jabri experimental tests was a load applied vertically to the beams at a distance of approximately 1,5 m from the centreline of the column web (Al-Jabri, 1999). Figure 3.5 illustrates the forces and moments acting on the joint, as a result of such loading configuration.

$M_{b1, Ed}$ Bending moment (right beam)

$M_{b2, Ed}$ Bending moment (left beam)

$V_{b1, Ed}$ Shear force (right beam)

$V_{b1, Ed}$ Shear force (left beam)

Figure 3.5: Forces and moments acting on the joint.

Eurocode EC 1993-1-8 provides guidance on the use of the component method for the prediction of the moment-rotation relationship of the bolted endplate beam-to-column joint. According to the joint configuration and the loading conditions explained above, the end-plate joint is assumed to be divided into three major zones: tension, compression and shear, as shows Figure 3.6. Within each zone, a number of components are specified, which contribute to the overall deformation and capacity of the joint. Each of these basic components possesses its own initial stiffness and contributes to the moment-rotation characteristic.
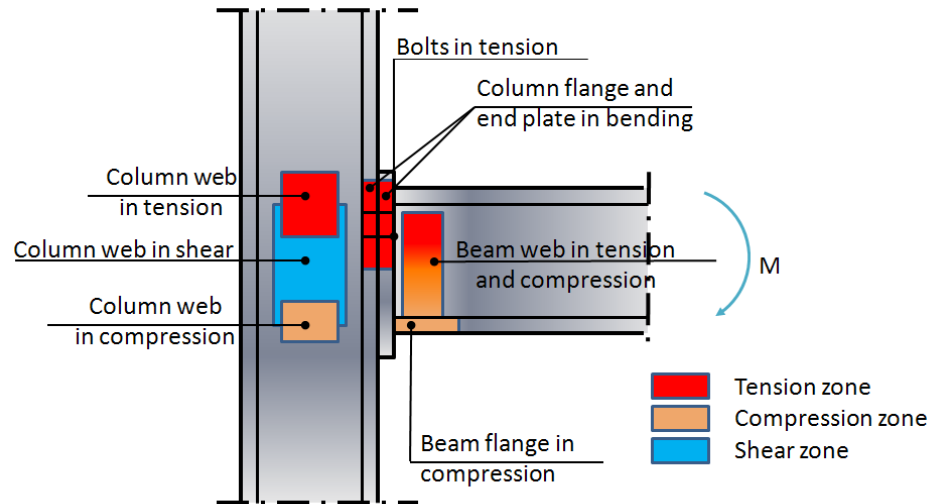
Figure 3.6: *Basic components of a beam-to-column joint in bending.*
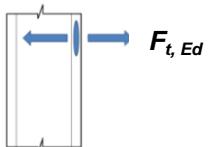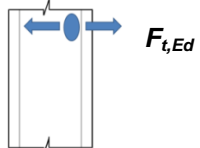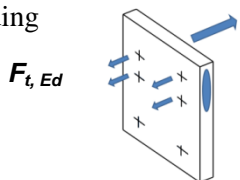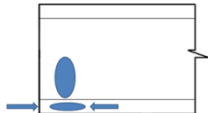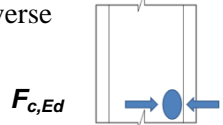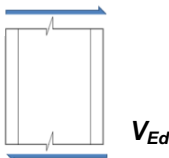
In the following sections the component method is applied to the studied case. The moment-rotation characteristic of the joint is obtained by assessing the Moment Design Resistance and the Rotational Stiffness. The numerical results determined for ambient temperature were used to verify the FEM model, as no experimental values were available for these conditions.

The material properties used for the calculations are defined according to the material properties of the steel used experimentally (Al-Jabri, 1999). The nominal material properties of the joint components are shown in Table 3.1. All components and design resistances which form the studied case according to the component method are summarized in Table 3.2. The following sections describe the mechanical characteristics of each component.

Table 3.1: *Material properties.*

	Material type	Yield strength [N/mm^2]	Ultimate tensile strength [N/mm^2]	Young's modulus [kN/mm^2]
Column	Grade 43	322	454	197
Beam	Grade 43	322	454	197
End-plate	Grade 43	322	454	197
Bolts	Grade8.8	640	800	210

Table 3.2: *Basic components of the studied joint and their design resistances.*

TENSION COMPONENTS		
1. Bolts in tension $F_{t,Ed}$		$F_{t,Rd}$: Bolt tension resistance
2. Colum flange in bending $F_{t,Ed}$		$F_{t,fc,Rd}$: Column flange tension resistance in bending
3. Column web in transverse tension $F_{t,Ed}$		$F_{t,wc,Rd}$: Column web tension resistance
4. End-plate in bending $F_{t,Ed}$		$F_{t,ep,Rd}$: End plate tension resistance in bending
5. Beam web in tension $F_{t,Ed}$		$F_{t,wb,Rd}$: Beam web tension resistance
COMPRESSION COMPONENTS		
6. Beam flange and web in compression $F_{c,Ed}$		$F_{c,fb,Rd}$: Beam flange compression resistance
7. Column web in transverse compression $F_{c,Ed}$		$F_{c,wc,Rd}$: Column web compression resistance
SHEAR COMPONENTS		
8. Column web panel in shear V_{Ed} V_{Ed}		$V_{wp,Rd}$: Column web panel shear resistance

3.3.   Tension Design Resistances

3.3.1.   Bolts in tension

The design resistance for the individual bolts subjected to tension should be obtained from equation 3.1

$$F_{t,Rd} = \frac{k_2\, f_{ub}\, A_s}{\gamma_{M2}}$$

(3.1)

where

$F_{t,Rd}$ is the design tension resistance for one bolt,

k_2 is a factor which takes into account the type of bolt, $k_2 = 0,9$

f_{ub} is the ultimate tensile strength of the bolt, $f_{ub} = 800 \text{ N/mm}^2$

A_s is the tensile stress area of the bolt, $A_s = 157 \text{ mm}^2$

γ_{M2} is the partial safety factor for resistance of cross-sections in tension to fracture, $\gamma_{M2} = 1,0$

The design tension resistance for each bolt $F_{t,Rd}$, obtained from 3.1 is 113 kN.

3.3.2.   Column flange in bending

The design resistance and failure mode of a column flange in bending together with the associated bolts in tension should be taken as similar to those of an equivalent T-stub flange. The resistance is given by finding the effective length of the equivalent T-stub. The meaning of parameters m, e, p_1 and p_2 are represented in Figure 3.7.
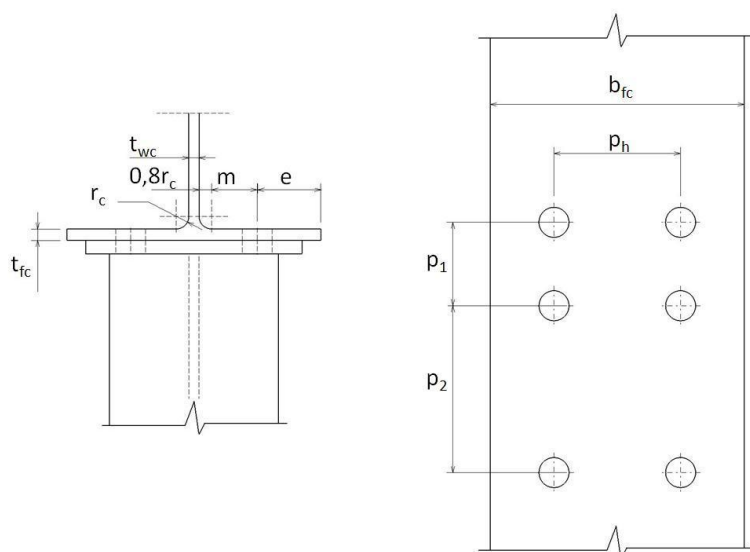
Figure 3.7*: Dimensions of the equivalent T-stub flange on column flange in bending.*

$m = (p_h - t_{wc})/2 - 0.8 r_c = 28,87$ mm

$e = (b_{fc} - p_h)/2 = 38,2$ mm

$p_1 = 50$ mm

$p_2 = 100$ mm

where

p_h is the horizontal spacing between holes,	$p_h = 76$ mm
t_{wc} is the thickness of the column web,	$t_{wc} = 6,1$ mm
r_c is the radius of the column section,	$r_c = 7,6$ mm
b_{fc} is the width of the column flange,	$b_{fc} = 152,4$ mm
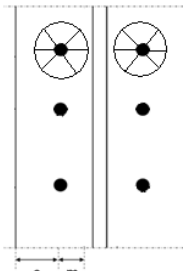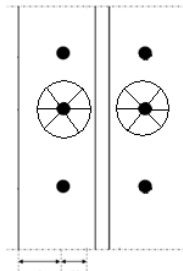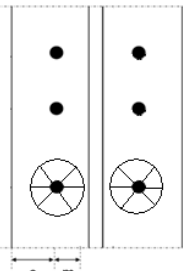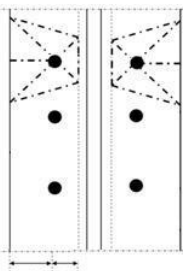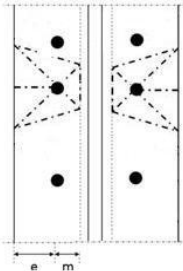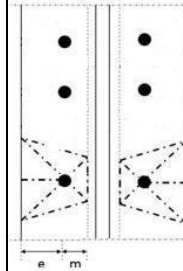
Column flange resistance has to be checked for each individual bolt row in tension and each individual group of bolt rows in tension according to EN 1993-1-8: 2005. This means that it has to be considered the effective lengths for bolt rows individually or as a group. Table 3.3 shows how the effective lengths for both assumptions are calculated according to circular yield mechanism and noncircular yield mechanism of the column flange.

Table 3.3 (a): *Effective lengths of the equivalent T-stub representing the column flange.* *Bolt rows considered individually.*

Circular patterns		
Bolt row 1	Bolt row 2	Bolt row 3
$l_{eff,cp} = 2\pi m = 181,4$ mm	$l_{eff,cp} = 2\pi m = 181,4$ mm	$l_{eff,cp} = 2\pi m = 181,4$ mm
Noncircular patterns		
Bolt row 1	Bolt row 2	Bolt row 3
$l_{eff,nc} = 4m + 1,25e = 163,2$ mm	$l_{eff,nc} = 4m + 1,25e = 163,2$ mm	$l_{eff,nc} = 4m + 1,25e = 163,2$ mm

Table 3.3 (b): *Effective lengths of the equivalent T-stub representing the column flange.*
Bolt rows considered as part of a group.

Circular patterns		
Group 1+2	Group 2+3	Group 1+2+3
$l_{eff,cp}=2(\pi m+p_1)=$ 281,395 mm	$l_{eff,cp}=2(\pi m+p_2)=$ 381,395 mm	$l_{eff,cp}=2\pi m+2p_1+2p_2=$ 481,395 mm
1) $\pi m+p_1=$140,69mm	**2)** $\pi m+p_2$=190,69mm	**1)** $\pi m+p_1=$ 140,69mm
2) $\pi m+p_1$=140,69 mm	**3)** $\pi m+p_2$=190,69mm	**2)** $p_1+p_2=$ 150 mm
		3) $\pi m+p_2=$ 190,69 mm
Noncircular patterns		
Group 1+2	Group 2+3	Group 1+2+3
$l_{eff,nc}=2(2m+0,625e+0,5p_1)=$ 213,23 mm	$l_{eff,nc}=2(2m+0,625e+0,5p_2)=$ 263,23 mm	$l_{eff,nc}=4m+1,25e+p_1+p_2=$ 313,23 mm
1) $2m+0,625e+0,5p_1=$ 106,615 mm	**2)** $2m+0,625e+0,5p_2=$ 131,615 mm	**1)** $2m+0,625e+0,5p_1=$ 106,615 mm
2) $2m+0,625e+0,5p_1=$ 106,615 mm	**3)** $2m+0,625e+0,5p_2=$ 131,615 mm	**2)** $0,5p_1+0,5p_2=$ 75 mm
		3) $2m+0,625e+0,5p_2=$ 131,615 mm

EN 1993-1-8: 2005 calculates the design resistance for column flange in bending using the equivalent T-stub, with the following proceeding.

The effective lengths of T-stub for the different failure modes are given by equation 3.2 for mode 1 and equation 3.3 for mode 2.

$$l_{eff.1} = l_{eff,nc} \text{ but } l_{eff.1} \leq l_{eff,cp} \tag{3.2}$$

$$l_{eff.2} = l_{eff,nc} \tag{3.3}$$

The plastic moment resistance for failure mode i is obtained with the expression 3.4

$$M_{pl,i,Rd} = \frac{0.25 \, l_{eff,i} \, t_f^2 \, f_{yc}}{\gamma_{M0}} \tag{3.4}$$

where

$M_{pl,i,Rd}$ is the plastic moment resistance of the failure mode i,

$l_{eff,i}$ is the effective length for the failure mode i,

t_f is the thickness of the column flange, $\qquad t_f = 6.8$ mm

f_{yc} is the column yield strength, $\qquad f_{yc} = 322$ N/mm^2

γ_{M0} is the partial safety factor for resistance of cross-sections, $\quad \gamma_{M0} = 1.0$

The design tension resistance $F_{T,Rd}$ is determined for each failure mode using expressions 3.5 - 3.7

Mode 1: complete yielding of the flange

$$F_{T,1,Rd} = \frac{4M_{pl,1,Rd}}{m} \tag{3.5}$$

Mode 2: Bolt failure with yielding of the flange

$$F_{T,2,Rd} = \frac{2M_{pl,2,Rd} + n \sum F_{t,Rd}}{m + n} \tag{3.6}$$

where $n = e_{min}$ but $n \leq 1.25m \rightarrow n = (b_p - p_h)/2 = 27$ mm

Mode 3: Bolt failure

$$F_{T,3,Rd} = \sum F_{t,Rd} \tag{3.7}$$

where $\sum F_{t,Rd}$ is the total sum of bolt tension resistances on the row (the tension resistance for each bolt $F_{t,Rd}$, is 113 kN).

Tables 3.4 and 3.5 summarize the results obtained.

Table 3.4: *Effective lengths and plastic moment resistances.*

	$l_{eff.1}$	$l_{eff.2}$	$M_{pl,1,Rd}$	$M_{pl,2,Rd}$
Bolt row 1	163 mm	163 mm	607,6 Nm	607,6 Nm
Bolt row 2	163 mm	163 mm	607,6 Nm	607,6 Nm
Group bolt rows 1+2	213 mm	213 mm	793,7 Nm	793,7 Nm
Bolt row 3	163 mm	163 mm	607,6 Nm	607,6 Nm
Group bolt rows 2+3	263 mm	263 mm	979,8 Nm	979,8 Nm
Group bolt rows 1+2+3	313 mm	313 mm	1165,9 Nm	1165,9 Nm

Table 3.5: *Tension resistances on each failure mode.*

	$F_{T,1,Rd}$	$F_{T,2,Rd}$	$F_{T,3,Rd}$
Bolt row 1	84,2 KN	131,0 KN	226,0 KN
Bolt row 2	84,2 KN	131,0 KN	226,0 KN
Group bolt rows 1+2	109,9 KN	246,9 KN	452,1 KN
Bolt row 3	84,2 KN	131,0 KN	226,0 KN
Group bolt rows 2+3	135,7 KN	253,6 KN	452,1 KN
Group bolt rows 1+2+3	161,5 KN	369,5 KN	678,2 KN

The design tension resistance for column flange in bending on individual bolt rows and group of bolt rows is calculated from expression 3.8 as the minimum of the three mode values.

$$F_{t,Rd} = Min\ (F_{T,1,Rd};\ F_{T,2,Rd};\ F_{T,3,Rd}) \tag{3.8}$$

The design tension resistance obtained for every case corresponds to failure mode 1 ($F_{T,1,Rd}$, complete yielding of the flange) with noncircular patterns.

3.3.3. Column web in transverse tension

The design resistance of a column web in tension is determined with the equation 3.9

$$F_{t,wc,Rd} = \frac{\omega\ b_{eff,t,wc}\ t_{wc}\ f_{y,wc}}{\gamma_{M0}} \tag{3.9}$$

where

$F_{t,wc,Rd}$ is the design resistance on tension for a column web,

$b_{eff,t,wc}$ should be taken as equal to the effective length of equivalent T-stub representing the column flange,

t_{wc} is the thickness of the column web, $\qquad\qquad t_{wc} = 6.1$ mm

f_{yc} is the column yield strength, $\qquad\qquad\qquad\qquad\quad$ $f_{yc} = 322$ N/mm^2

γ_{M0} is the partial safety factor for resistance of cross-sections, $\quad$ $\gamma_{M0} = 1,00$

ω is a reduction factor to allow the interaction with shear in the column web panel. Its value depends on the transformation parameter β.

The studied case is a symmetric joint configuration both geometrically and in action as shows Figure 3.8. This type of joint configuration with same value of moments acting on the web panel at both sides of the joint represents a value of $\beta = 0$.
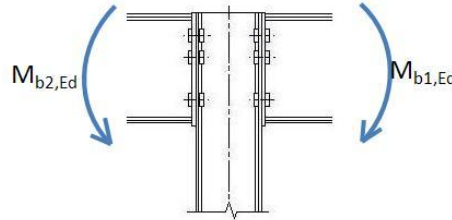
Figure 3.8: *Symmetric joint configuration ($M_{b1,Ed} = M_{b2,Ed}$).*

From EN 1993-1-8: 2005, a value of the transformation parameter $\beta = 0$ gives a reduction factor for interaction with shear $\omega = 1$.

The column web design resistances in transverse tension $F_{t,wc,Rd}$, obtained from 3.9

Bolt row 1: $b_{eff,t,wc} = l_{eff} = 163$ mm $\rightarrow$ $F_{t,wc,Rd} = 320,6$ KN.

Bolt row 2: $b_{eff,t,wc} = l_{eff} = 163$ mm $\rightarrow$ $F_{t,wc,Rd} = 320,6$ KN.

Group bolt rows 1+2: $b_{eff,t,wc} = l_{eff} = 213$ mm $\rightarrow$ $F_{t,wc,Rd} = 418,8$ KN.

Bolt row 3: $b_{eff,t,wc} = l_{eff} = 163$ mm $\rightarrow$ $F_{t,wc,Rd} = 320,616$ KN.

Group bolt rows 2+3: $b_{eff,t,wc} = l_{eff} = 263$mm $\rightarrow$ $F_{t,wc,Rd} = 517,0$ KN.

Group bolt rows 1+2+3: $b_{eff,t,wc} = l_{eff} = 313$ mm $\rightarrow$ $F_{t,wc,Rd} = 615,2$ KN.

3.3.4. End plate in bending

The design resistance and failure mode of the end plate in bending, together with the associated bolts in tension, should be taken as similar to those of an equivalent T-stub flange, as happened with column flange in bending. For the modelling of an endplate as separate T-stubs the parameters e, m, p_1 and p_2 are needed. Figure 3.9 represents them for the studied case.
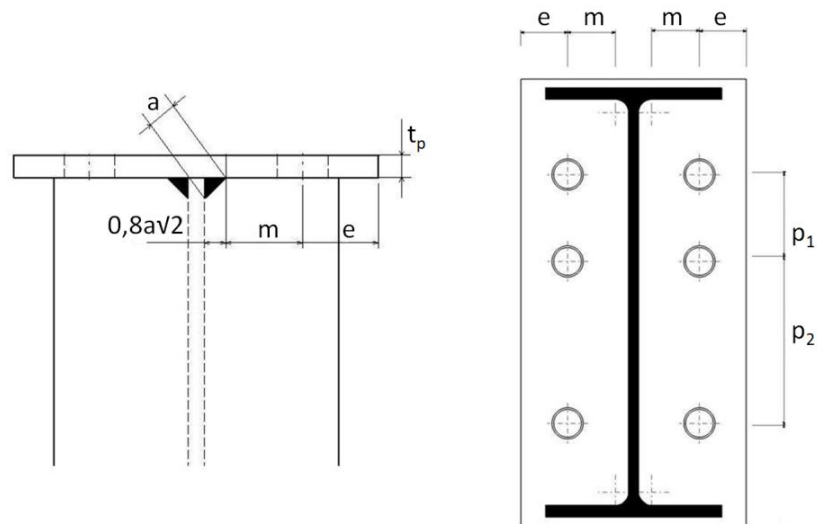
Figure 3.9: *Dimensions of the equivalent T-stub flange on end-plate in bending.*

$m = (p_h - t_{wb})/2 - 0,8a\sqrt{2} = 30,57$ mm

$e = (b_p - p_h)/2 = 27$ mm

$p_1 = 50$ mm

$p_2 = 100$ mm

where

p_h is the horizontal spacing between holes,	$p_h = 76$ mm
t_{wb} is the beam web thickness,	$t_{wb} = 5,8$ mm
a is the web weld thickness,	$a = 4$mm
b_p is the thickness of the endplate,	$b_p = 8$ mm
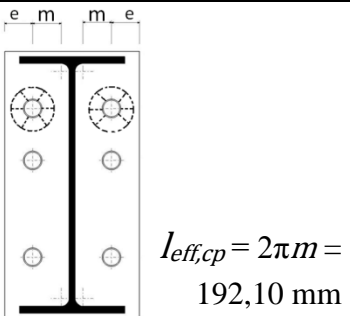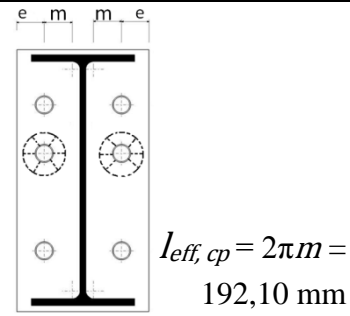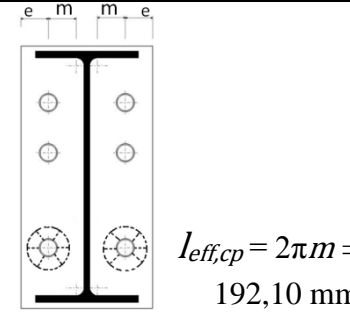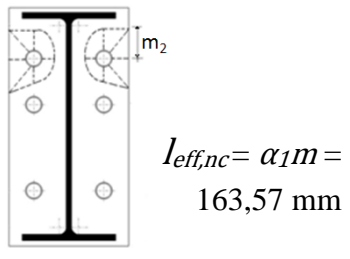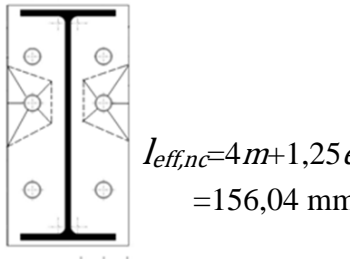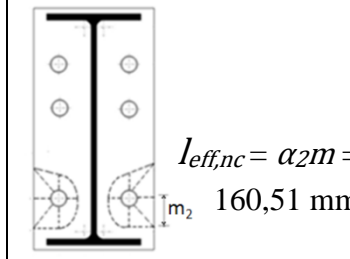
The effective lengths for the end-plate in bending are determined using EN 1993-1-8: 2005. As it happened with the column flange, they must be considered for bolt rows individually or as a group. Table 3.6 shows the effective lengths in circular yield mechanism and noncircular yield mechanism for the equivalent T-stub flange at the studied case.

Table 3.6 (a): *Effective lengths for of the equivalent T-stub representing the endplate. Bolt rows considered individually.*

Circular patterns		
Bolt row 1	**Bolt row 2**	**Bolt row 3**
$l_{eff,cp} = 2\pi m = 192{,}10$ mm	$l_{eff,\,cp} = 2\pi m = 192{,}10$ mm	$l_{eff,cp} = 2\pi m = 192{,}10$ mm
Noncircular patterns		
Bolt row 1	**Bolt row 2**	**Bolt row 3**
$l_{eff,nc} = \alpha_1 m = 163{,}57$ mm	$l_{eff,nc} = 4m + 1{,}25e = 156{,}04$ mm	$l_{eff,nc} = \alpha_2 m = 160{,}51$ mm

Yielding line factors α_1 and α_2 appear for the bolt rows adjacent to the beam flanges. To obtain them the parameters λ_1 and λ_2 are assessed from expressions 3.10 and 3.11

$$\lambda_1 = \frac{m}{m+e} \tag{3.10}$$

$$\lambda_2 = \frac{m_2}{m+e} \tag{3.11}$$

where
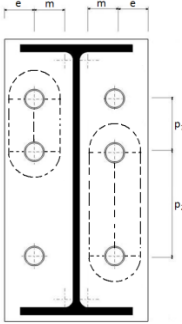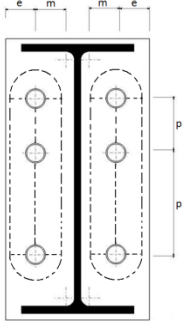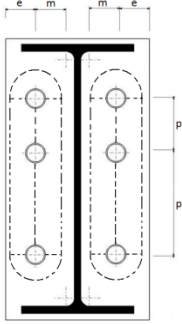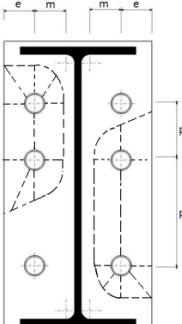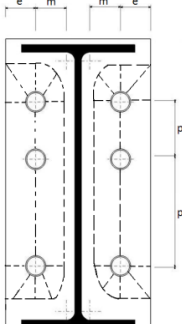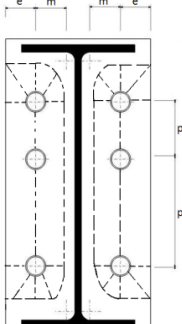
m_2 is the vertical distance between the bolt row and beam flange. It is represented on figure 3.10, and its value is 37,12 mm for the first bolt row and 41,12 mm for the third bolt row.
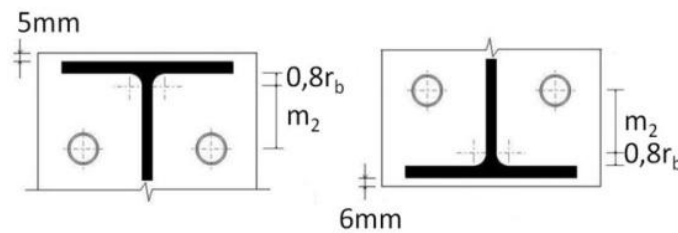
Figure 3.10: *Dimensions of the end-plate in bending.*

The values obtained for yielding line factors α_1 and α_2 are 5,35 and 5,25 respectively.

Table 3.6 (b): *Effective lengths for of the equivalent T-stub representing the endplate.* *Bolt rows considered as part of a group.*

Circular patterns		
Group 1+2	Group 2+3	Group 1+2+3
$l_{eff,cp}=2(\pi m+p_1)=292,1$ mm	$l_{eff,cp}=2(\pi m+p_2)=392,1$mm	$l_{eff,cp} = 2\pi m + 2p_1+2p_2=481,39$mm
1) $\pi m+p_1 = 146,05$ mm	**2)** $\pi m+p_2 = 196,05$ mm	**1)** $\pi m + p_1 = 140,69$ mm
2) $\pi m+p_1 = 146,05$ mm	**3)** $\pi m+p_2 = 196,05$ mm	**2)** $p_1 + p_2 = 150$ mm
		3) $\pi m + p_2 = 190,69$ mm
Noncircular patterns		
Group 1+2	Group 2+3	Group 1+2+3
$l_{eff,nc}=\alpha_1 m +p_1 = 213,57$mm	$l_{eff,nc}=\alpha_2 m + p_2 = 206,51$mm	$l_{eff,nc}=\alpha_1 m+\alpha_2 m-(4m+1,25e)+p_1+p_2 =318,04$mm
1) $\alpha_1 + 0,5p_1 - (2m + 0,625e) = 110,54$ mm	**2)** $2m + 0,625 + 0,5p_2 = 128,024$mm	**1)** $\alpha_1 m + 0,5p_1 - (2m + 0,625e) = 110,54$mm
2) $2m+0,625e+0,5p_1 = 103,024$mm	**3)** $\alpha_2 m+0,5p_2-(2m+0,625e)=132,492$mm	**2)** $0,5p_1+0,5p_2 = 75$ mm
		3) $\alpha_2 m+ 0,5p_2-(2m+0,625e)=132,492$mm

The equivalent T-stub method (EN 1993-1-8: 2005) is used to determine the design resistance. The proceeding is same as for column flange.

The effective lengths of T-stub for the different failure modes are given by equation 3.12 for mode 1 and equation 3.13 for mode 2.

$$l_{eff.1} = l_{eff,nc} \text{ but } l_{eff.1} \le l_{eff,cp} \tag{3.12}$$

$$l_{eff.2} = l_{eff,nc} \tag{3.13}$$

The plastic moment resistance for failure mode i is obtained with the expression 3.14.

$$M_{pl,i,Rd} = \frac{0{,}25 \, l_{eff,i} \, t_p^2 \, f_{yp}}{\gamma_{M0}} \tag{3.14}$$

where

$M_{pl,i,Rd}$ is the plastic moment resistance of the failure mode i,

$l_{eff,i}$ is the effective length for the failure mode i,

t_p is the thickness of the end-plate, $\qquad\qquad\qquad t_p = 8$ mm

f_{yp} is the end-plate yield strength, $\qquad\qquad\qquad f_{yc} = 322$ N/mm^2

γ_{M0} is the partial safety factor for resistance of cross-sections, $\qquad \gamma_{M0} = 1{,}00$

The design tension resistance $F_{T,Rd}$ is determined for each failure mode using expressions 3.5 - 3.7.

Tables 3.7 and 3.8 summarize the results obtained.

Table 3.7: *Effective lengths and plastic moment resistances.*

	$l_{eff,1}$	$l_{eff,2}$	$M_{pl,1,Rd}$	$M_{pl,1,Rd}$
Bolt row 1	163 mm	163 mm	842,7 Nm	842,7 Nm
Bolt row 2	156 mm	156 mm	803,9 Nm	803,9 Nm
Group bolt rows 1+2	213 mm	213 mm	1100,3 Nm	1100,3 Nm
Bolt row 3	160 mm	160 mm	827 Nm	827 Nm
Group bolt rows 2+3	260 mm	260 mm	1342,1 Nm	1342,1 Nm
Group bolt rows 1+2+3	318 mm	318 mm	1638,5 Nm	1638,5 Nm

Table 3.8: *Tension resistances on each failure mode.*

	$F_{T,1,Rd}$	$F_{T,2,Rd}$	$F_{T,3,Rd}$
Bolt row 1	110,2 KN	135,3 KN	226,0 KN
Bolt row 2	105,2 KN	135,3 KN	226,0 KN
Group bolt rows 1+2	143,9 KN	250,3 KN	452,1 KN
Bolt row 3	108,19 KN	134,7 KN	226,0 KN
Group bolt rows 2+3	175,6 KN	258,7 KN	452,1KN
Group bolt rows 1+2+3	214,3 KN	375 KN	678,2 KN

The design tension resistance for end-plate in bending on individual bolt rows and group of bolt rows is obtained from expression 3.15 as the minimum of the three mode values.

$$F_{t,Rd} = Min \ (F_{T,1,Rd}; \ F_{T,2,Rd}; \ F_{T,3,Rd}) \qquad (3.15)$$

The design tension resistance obtained for every case corresponds to failure mode 1 ($F_{T,1,Rd}$, complete yielding of the flange) with noncircular patterns.

3.3.5. Beam web in tension

The design tension resistance of the beam web should be obtained with the equation 3.16

$$F_{t,wb,Rd} = \frac{b_{eff,t,wb} \ t_{wb} \ f_{y,wb}}{\gamma_{M0}} \qquad (3.16)$$

where

$F_{t,wb,Rd}$ is the design resistance on tension for a beam web,

$b_{eff,t,wc}$ should be taken as equal to the effective length of equivalent T-stub representing the end-plate,

t_{wb} is the beam web thickness, $\hspace{3cm} t_{wb} = 5{,}8$ mm

$f_{y,wb}$ is the beam yield strength, $\hspace{3cm} f_{y,wb} = 322$ N/mm^2

γ_{M0} is the partial safety factor for resistance of cross-sections, $\hspace{1cm} \gamma_{M0} = 1{,}00$

The beam web design resistances in tension $F_{t,wb,Rd}$, obtained from 3.16

Bolt row 1: $b_{eff,t,wc} = l_{eff} = 163$ mm ➔ $F_{t,wb,Rd} = 305{,}4$ KN.

Bolt row 2: $b_{eff,t,wc} = l_{eff} = 156$ mm ➔ $F_{t,wb,Rd} = 291{,}4$ KN.

Group bolt rows 1+2: $b_{eff,t,wc} = l_{eff} = 213$ mm ➔ $F_{t,wb,Rd} = 398{,}9$ KN.

Bolt row 3: $b_{eff,t,wc} = l_{eff} = 160$ mm ➔ $F_{t,wb,Rd} = 299{,}8$ KN.

Group bolt rows 2+3: $b_{eff,t,wc} = l_{eff} = 260$ mm ➔ $F_{t,wb,Rd} = 486{,}5$ KN.

Group bolt rows 1+2+3: $b_{eff,t,wc} = l_{eff} = 318$ mm ➔ $F_{t,wb,Rd} = 594$ KN.

3.4. Compression Design resistances

3.4.1. Beam flange and web in compression

The resultant of the design compression resistance of a beam flange and the adjacent compression zone of the beam web may be assumed to act at the level of the centre of compression. In the studied case this centre of compression is in line with the mid-thickness of the compression flange, as shows Figure 3.11.
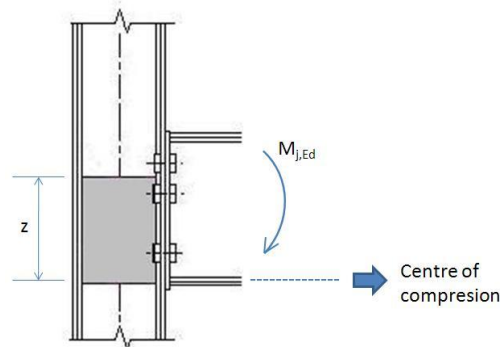
Figure 3.11: *Centre of compression.*

The design compression resistance of the combined beam flange and web is given by the expression 3.17.

$$F_{c,fb,Rd} = \frac{M_{c,Rd}}{(h_b - t_{fb})}$$
(3.17)

where

$F_{c,fb,Rd}$ is the design compression resistance,

h_b is the height of the beam, $\qquad\qquad h_b = 254$ mm

t_{fb} is the thickness of the beam flange, $\qquad t_{fb} = 6,8$ mm

$M_{c,Rd}$ is the design moment resistance for bending of the beam cross-section, and from EN 1993-1-1: 2005 it is determined with the equation 3.18.

$$M_{c,Rd} = M_{pl,Rd} = \frac{W_{pl}\, f_{yb}}{\gamma_{M0}}$$
(3.18)

where

W_{pl} is the plastic section modulus of the beam, $\qquad W_{pl} = 260,00$ cm^2

f_{yb} is the beam yield strength, $\qquad\qquad f_{yb} = 322$ N/mm^2

γ_{M0} is the partial safety factor for resistance of cross-sections, $\gamma_{M0} = 1,0$

The design moment resistance $M_{c,Rd}$, obtained from 3.18 is 83,72 KNm. The design resistance for beam flange and web in compression $F_{c,fb,Rd}$, obtained from 3.17 is 338,7 KN.

3.4.2. Column web in transverse compression

The design resistance of an unstiffened column web subject to transverse compression should be determined from 3.19

$$F_{C,wc,Rd} = \frac{\omega k_{wc}\, b_{eff,c,wc}\, t_{wc}\, f_{y,wc}}{\gamma_{M0}} \quad \text{but} \quad F_{C,wc,Rd} \leq \frac{\omega k_{wc}\, \rho\, b_{eff,c,wc}\, t_{wc}\, f_{y,wc}}{\gamma_{M1}} \quad (3.19)$$

where

$F_{C,wc,Rd}$ is the design resistance for column web in compression,

ω is a reduction factor to allow the possible effects of interaction with shear in the column web panel. It is determined as in column web in transverse tension case. $\hspace{2cm} \omega = 1$

k_{wc} is a reduction factor, $\hspace{4cm} k_{wc} = 1$

t_{wc} is the thickness of the column web, $\hspace{2.5cm} t_{wc} = 6{,}1$ mm

$f_{y,wc}$ is the column yield strength, $\hspace{2.5cm} f_{y,wc} = 322$ N/mm^2

$b_{eff,c,wc}$ is the effective width of column web in compression for bolted end-plate joint. It can be calculated from equation 3.20

$$b_{eff,c,wc} = t_{fb} + 2\sqrt{2}a_p + 5(t_{fc} + s) + s_p \hspace{2cm} (3.20)$$

where

t_{fb} is the beam flange thickness, $\hspace{3cm} t_{fb} = 6{,}8$ mm

a_p is the flange weld thickness, $\hspace{3.2cm} a_p = 3$ mm

t_{fc} is the column flange thickness, $\hspace{2.7cm} t_{fc} = 6{,}8$ mm

$s = r_c$ is the radius of the column section, $\hspace{2cm} r_c = 7{,}6$ mm

s_p is the length obtained by dispersion at 45° through the end plate,

$\hspace{8cm} s_p = 6+8 = 14$ mm

These values are shown on Figure 3.12.
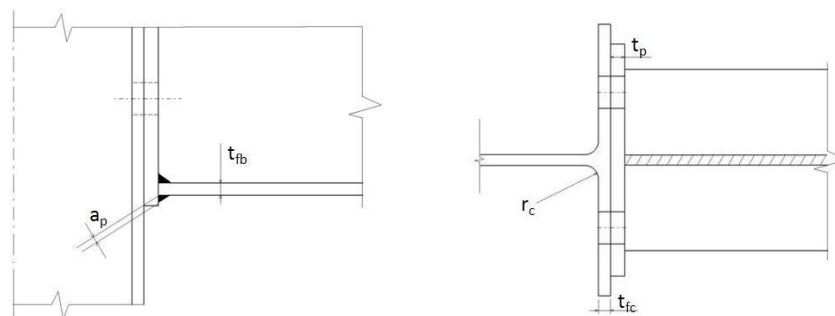
Figure 3.12*: Dimensions for effective width of column web in compression.*

The effective width $b_{eff,c,wc}$, obtained from 3.20 is 97,04 mm.

ρ is the reduction factor for plate buckling. It depends on the plate slenderness, which is assessed from expression 3.21

$$\lambda_p = 0{,}932 \sqrt{\frac{b_{eff,c,wc}\, d_{wc}\, f_{y,wc}}{E t_{wc}^2}} \tag{3.21}$$

where

$b_{eff,c,wc}$ is the effective width

E is Young's modulus of the end-plate $\qquad E = 197$ KN/mm^2

d_{wc} is the clear depth of the column web $\qquad d_{wc} = 123{,}6$ mm

The plate slenderness λ_p, obtained from 3.21 is 0,676, so reduction factor ρ is 1,0 ($\lambda_p \leq$ 0,72).

The design resistance for column web in compression $F_{C,wc,Rd}$, obtained from 3.19 is 190,6 kN.

3.5. Shear Design Resistance

3.5.1. Column web panel in shear

The design plastic shear resistance $V_{wp,Rd}$ of the column web panel should be obtained from the equation 3.22

$$V_{wp,Rd} = \frac{0{,}9\, f_{y,wc}\, A_{vc}}{\sqrt{3}\gamma_{M0}} \tag{3.22}$$

where

$V_{wp,Rd}$ is the design shear resistance of the column web panel,

$f_{y,wc}$ is the column yield strength, $\qquad\qquad f_{y,wc} = 322$ N/mm^2

A_{vc} is the shear area of the column $\quad A_{vc}=A_c\text{-}2b_c\, t_{fc}+(t_{wc}\text{-}2r_c)t_{fc} = 8{,}3548$ cm^2

γ_{M0} is the partial safety factor for resistance of cross-sections, $\qquad \gamma_{M0} = 1{,}0$

The design plastic shear resistance for the column web $V_{wp,Rd}$, obtained from 3.22 is 139,8 kN.

3.6. Assembly of Components and Design Resistances

The failure mechanism of the joint will be controlled by the weakest component in the model. From the calculations above, it is possible to determine which are the limiting component resistances of the joint. On every bolt row the failure can be reached in a different component, with a different magnitude of resistance, and failure mode. Table 3.9 shows the limiting component design resistances resultant to the case of study.

Table 3.9: Limiting components and design resistances.

Row	Component	F_{Rd}
1	Column flange in transverse bending	**84,18kN**
2	Column flange in transverse bending (group of bolt rows 1+2)	109,97-84,18 = **25,8kN**
3	Column flange in transverse bending (group of bolt rows 1+2+3)	161,54-84,18-25,78 = **51,6kN**

3.7. Structural properties

As it was previously said, the structural properties of a semi-rigid joint is represented by the moment-rotation behaviour. By determining the Design Moment Resistance and the Rotational Stiffness, the moment-rotation characteristics of the joint is established. For the case of semi-rigid joints the moment-rotation relationship can be represented using one of the simplifications showed in Figure 3.13 (EN 1993-1-8, 2005).
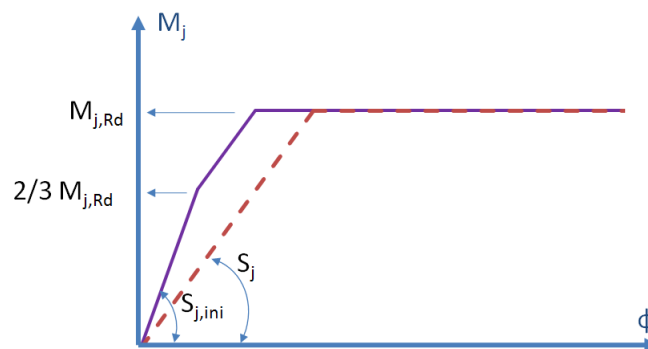
Figure 3.13: Moment-rotation relationship (EN 1993-1-8, 2005). $M_{j,Rd}$: Design Moment Resistance, S_j: Rotational Stiffness, $S_{j,ini}$: Initial Rotational Stiffness.

3.7.1. Design moment resistance

The design moment resistance may be determined from expression 3.23

$$M_{j,Rd} = \sum h_r F_{tr,Rd} \qquad (3.23)$$

where

$M_{j,Rd}$ is the design moment resistance,

$F_{tr,Rd}$ is the effective design tension resistance of bolt-row r;

$F_{t1,Rd} = 84{,}18$ kN

$F_{t2,Rd} = 25{,}78$ kN

$F_{t3,Rd} = 51{,}57$ kN

h_r is the distance from bolt-row r to the centre of compression. The centre of compression is located at the mid line of the bottom flange of the beam.

$h_1 = 200{,}6$ mm

$h_2 = 150{,}6$ mm

$h_3 = 50{,}6$ mm

r is the bolt-row number.

The design moment resistance $M_{j,Rd}$, obtained from 3.23, which can be defined as the maximum moment that the studied joint is able to resist following the Component Method:

$M_{j,Rd} = 23{,}38$ kNm

3.7.2. Rotational stiffness

The rotational stiffness of the joint is determined from the flexibilities of its components, each represented by an elastic stiffness coefficient k_i. According to EN 1993-1-8, 2005 for a joint with bolted end-plate joint double sided with moments equal and opposite, and more than one bolt-row in tension, the stiffness coefficients k_i needed to determine the rotational stiffness are k_2 and k_{eq}.

where

k_2 is the stiffness coefficient for column web in compression,

k_{eq} is the equivalent stiffness coefficient related to the bolt rows in tension.

The stiffness coefficients for a joint's components should be determined using the expressions given in Table 3.10 based on EN 1993-1-8, 2005.

Table 3.10: *Components' stiffness coefficients.*

Column web in compression		
$k_2 = \dfrac{0,7 b_{eff,c,wc} t_{wc}}{dc}$	$b_{eff,c,wc}$ is the effective width of column web in compression, $b_{eff,c,wc} = 97{,}042$ mm t_{wc} is the thickness of the column web, $t_{wc} = 6{,}1$ mm d_c is the clear depth of the column web, $d_c = 123{,}6$ mm	k_2=3,35mm
Column web in tension		
$k_3 = \dfrac{0,7 b_{eff,t,wc} t_{wc}}{dc}$	$b_{eff,t,wc}$ is the effective width of the column web in tension (*) $t_{wc} = 6{,}1$ mm $d_c = 123{,}6$ mm	
	Bolt row 1 · $b_{eff,t,wc}$=106,615mm	$k_{3,1}$=3,68mm
	Bolt row 2 · $b_{eff,t,wc}$=75mm	$k_{3,2}$=2,59mm
	Bolt row 3 · $b_{eff,t,wc}$=131,615mm	$k_{3,3}$=4,55mm
Column flange in bending		
$k_4 = \dfrac{0,9 l_{eff} t_{fc}{}^3}{m^3}$	t_{fc} is the thickness of the column flange, $t_{fc} = 6{,}8$ mm m is the horizontal distance from the bolts to the column web, m=28,87 mm l_{eff} is the smallest of the effective lengths (*)	
	Bolt row 1 · $l_{eff} = 106{,}615$mm	$k_{4,1}$=1,25mm
	Bolt row 2 · $l_{eff} = 75$mm	$k_{4,2}$=0,88mm
	Bolt row 3 · $l_{eff} = 131{,}615$mm	$k_{4,3}$=1,55mm
End plate in bending		
$k_5 = \dfrac{0,9 l_{eff} t_p{}^3}{m^3}$	t_p is the thickness of the endplate, t_p=8mm m is the horizontal distance from the bolts to the beam web, m=30,57mm l_{eff} is the smallest of the effective length (*)	
	Bolt row 1 · $l_{eff} = 110{,}55$mm	$k_{5,1}$=1,78mm
	Bolt row 2 · $l_{eff} = 75$mm	$k_{5,2}$=1,21mm
	Bolt row 3 · $l_{eff} = 132{,}49$mm	$k_{5,3}$=2,14mm
Bolts in tension		
$k_{10} = 1,6\, A_s\, /\, L_b$	A_s is the tensile stress area of the bolts, $A_s = 157$ mm2 L_b is the bolt elongation length (**)	
	Bolt row 1 · $L_b = 26{,}3$ mm	$k_{10,1}$=9,5mm
	Bolt row 2 · $L_b = 26{,}3$ mm	$k_{10,2}$=9,5mm
	Bolt row 3 · $L_b = 26{,}3$ mm	$k_{10,3}$=9,5mm

(*) Individually or as part of a group of bolts.

(**) The bolt elongation, represented on figure 3.14, may be obtained from the relationship expressed on 3.24

$$L_b = t_p + t_{cf} + \frac{t_{bh} + t_{bn}}{2} \tag{3.24}$$

where (estimated for M16 bolts)

L_b is the bolt elongation length,

t_p is the thickness of the endplate,	$t_p = 8$ mm
t_{cf} is the thickness of the column flange,	$t_{cf} = 6{,}8$ mm
t_{bh} is the thickness of the bolt head,	$t_{bh} = 10$ mm
t_{bn} is the thickness of the bolt nut,	$t_{bn} = 13$ mm
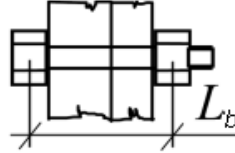
Figure 3.14: *Bolt elongation, L_b.*

The use of a single spring of equivalent stiffness permits to represent the stiffness of the springs in the tension zone where there is more than one bolt row in tension. The equivalent stiffness coefficient k_{eq}, is assessed from the expression 3.25

$$k_{eq} = \frac{\sum_r k_{eff,r}\, h_r}{z_{eq}} \tag{3.25}$$

where

$k_{eff,r}$ is the effective coefficient for bolt row r. It represents the overall stiffness of the components in the tension zone at any bolt row, and may be expressed using equation 3.26. The values obtained for the three bolt rows of the studied case are represented on Table 3.11.

$$k_{eff,r} = \frac{1}{\sum \frac{1}{k_{i,r}}} \tag{3.26}$$

Table 3.11: *Effective coefficients for bolt rows.*

	Bolt row 1	Bolt row 2	Bolt row 3
k_3 (mm)	3,68	2,59	4,55
k_4 (mm)	1,25	0,88	1,55
k_5 (mm)	1,78	1,21	2,14
k_{10} (mm)	9,5	9,5	9,5
k_{eff} (mm)	$k_{eff,1} = 0{,}576$	$k_{eff,2} = 0{,}407$	$k_{eff,3} = 0{,}695$

h_r is the distance between bolt-row r and the centre of compression,

$h_1 = 200{,}6$ mm

$h_2 = 150{,}6$ mm

$h_3 = 50{,}6$ mm

z_{eq} is the equivalent lever arm. When considering the stiffness of the equivalent spring in the tension zone k_{eq}, it is necessary to determine the distance from the centre of compression to the location of the equivalent tension spring. For joints with more than one bolt row acting in tension the equivalent lever arm zeq may be calculated from expression 3.27

$$z_{eq} = \frac{\sum k_{eff,r}\, h_r^2}{\sum k_{eff,r}\, h_r} \tag{3.27}$$

Figure 3.15 shows the distances h_r described above, the effective springs for bolt rows, as well as the final equivalent spring system representing the joint behaviour, locating the equivalent spring stiffness for the tension zone at a distance from the centre of compression of the equivalent lever arm z_{eq}.
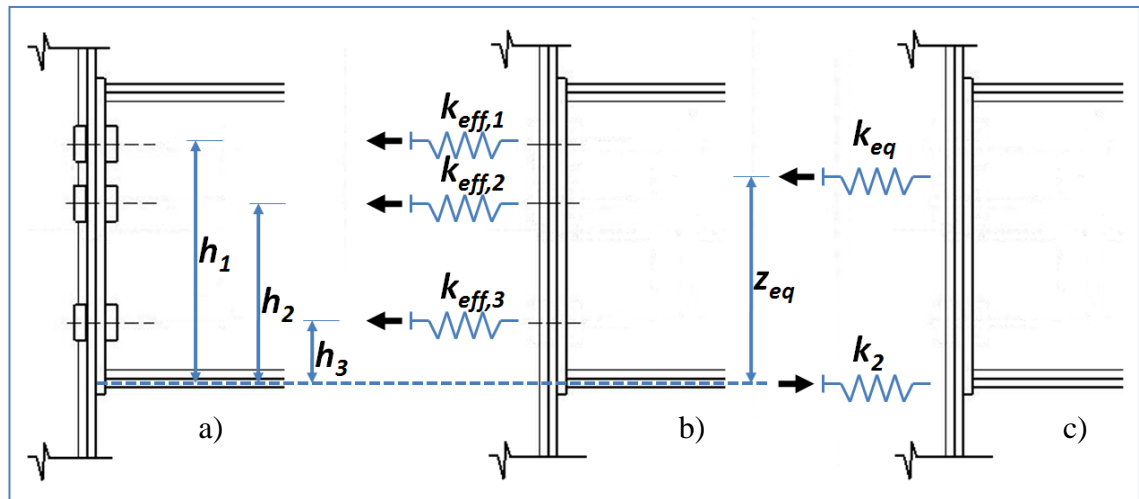
Figure 3.15: *Representation of the endplate beam-to-column joint using spring-stiffness model based on the component method.*

The equivalent lever arm z_{eq}, obtained from expression 3.27 is 161,27 mm. The equivalent stiffness coefficient k_{eq}, obtained from the expression 3.25 is 1,316 mm. The rotational stiffness for the structural joint of study S_j , may be obtained with sufficient accuracy from equation 3.28

$$S_j = \frac{E\, z_{eq}^2}{\eta\left(\frac{1}{k_2} + \frac{1}{k_{eq}}\right)} \tag{3.28}$$

where

E is the Young's modulus, E = 197 KN/mm2

z_{eq} is the equivalent lever arm, z_{eq} = 161,27 mm

η is the stiffness ratio $S_{j,ini}/S_j$ η =2

The rotational stiffness S_j, obtained from 2.28 and the initial rotational stiffness $S_{j,ini}$:

S_j = 2421 kNm / rad	$S_{j,ini}$ = 4842 kNm / rad

4. FEM ANALYSIS WITH ABAQUS

In order to analyse and understand the behaviour of beam-to-column joints at ambient and elevated temperatures, the Finite Element Method software ABAQUS/CAE 6.9 was used for the modelling of a bolted joint based on the fire tests performed on Al-Jabri *et al*.,1999. Simulating the joint behaviour via Finite Element modelling provides the opportunity of wider parametric investigations and eliminates some limitations asociated with experimental studies. Recently, different analytical models have been developed for the design of joints on fire conditions giving satisfactory results. Sarraj *et al.*, 2007 modelled finplate joints in fire using ABAQUS, in which surface to surface contact with small sliding was used. Yu *et al.*, 2008 developed numerical simulations using ABAQUS/Explicit solver to model bolted joints in order to enhance the numerous contact problems by controlling the time step.

4.1. Model Description

A three-dimensional (3-D) FE model of the endplate joint was developed on standard static analysis. The simulation of bolted steel joints becomes a challenging task, since contact models lead to convergence difficulties on static solvers. The contact interaction was carefully defined on the model during the first steps of the analysis. Only after full contact was established the loading was applied. The results were studied for validation against available test data and the component-based model developed on previous chapter.

4.1.1. Contact interaction

Large number of contacts exist in the model since the connection is a bolted joint. Numerical modelling of any joint requires a realistic representation of the contact interaction between the various components in order to allow the load to be transmited from one part of the model to another.

The contact which was established is shown on Figure 4.1. It was defined between bolts and endplates, bolts and column, as well as between column and endplates. The interaction at the contact parts of the model was defined as *surface-to-surface* contact with *finite sliding*. This contact formulation requires for ABAQUS a constant determination of which part of the master surface is in contact with each slave node; and it also becomes more complex if both contacting bodies are deformable (Dassault Systèmes Simulia, 2009).

a)   *b)*
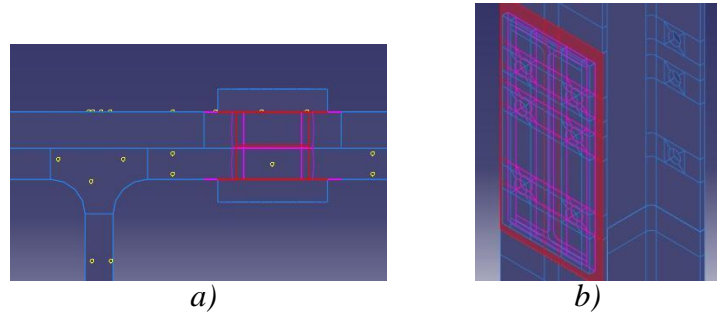
Figure 4.1: *Surface-to-surface contact. a) contact between bolt and endplate, contact between bolt and column. b) contact between endplate and column.*

At one bolt contact level it was defined three surfaces (Figure 4.2). One was the bolt surface, which comprises the bolt shank together with the inner surfaces of bolt head and nut; and then bolt holes at endplate and column with outter surfaces comprise the other two surfaces. By this surface configuration, it was established two contact interactions. Contact between bolt shanks-to-endplate bolt holes together with bolt heads-to-endplate; and the bolt shanks-to-column bolt holes together with nuts-to-column flanges. The bolt holes were modelled 2 mm larger than the bolt diameter, and the hexagon bolt heads were modelled as cylinders. To reduce the number of contact planes and the complexity of the model, the bolt nut forms an integral component with the bolt shank rather than as an individual part.
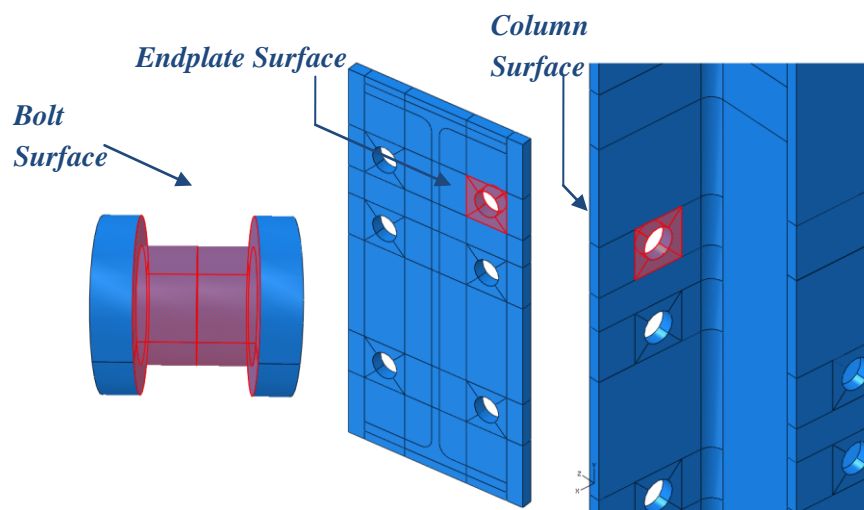
Figure 4.2*: Surfaces at one bolt contact level.*

The contact formulation used in ABAQUS involves a master-slave type algorithm. This kind of contact approach needs that one of the contact surfaces must be defined as *master* surface and the other as *slave* surface. The difference between them is on the algorithm restrictions. Nodes on slave surface cannot penetrate the segments that make up the master surface, while master surface can penetrate the slave surface between nodes (Dassault Systèmes Simulia, 2009). As a consequence, it is of great importance to carefully assign the slave and master surfaces. For choosing these surfaces, the rule which was followed on the model was to assign to stronger material bodies the master surfaces; or to the more finely meshed surfaces the slave surfaces. Table 4.1 shows which are the master and slave surfaces for the contact areas of the studied model.

Table 4.1*: Master and Slave surfaces.*

	Master Surface	**Slave surface**
Bolt Vs Column	Bolt	Column
Bolt Vs Endplate	Bolt	Endplate
Endplate Vs Column	Column	Endplate

For the tangential behaviour a friction coeffitient μ of 0,2 was adopted and for normal behaviour it was used *hard* contact. This is a contact property from ABAQUS which means that when the contact pressure between the contact surfaces becomes zero or negative, the constraint is removed and the surfaces separate (Dassault Systèmes Simulia, 2009).

Simulating the contact interaction between the parts of a shear joint using ABAQUS is a very sensitive and difficult issue to achieve, but it is of satisfactory accuracy when established. The diffculties arise because special arrangements are needed to bring the parts into initial contact. In the model developed for this thesis the contact was achieved by using thirteen steps.

1st *step*: All bolt heads are maintained away from contact. During this first step it is defined in every bolt a displacement of 0,1 mm in the opposite direction of contact as shows Figure 4.3 a. This guarantees that contact status would only be established on the following steps.

$2^{nd} - 13^{th}$ *step*: Every bolt is pulled to contact on the analysis as shows Figure 4.3 b, by using one step per bolt (12 bolts). In this case a small displacement of 1×10^{-5} mm is introducing into the model the contact at every bolt. The reason of not defining the contact at one step is to reduce the number of nodes changing contact status at the same time.
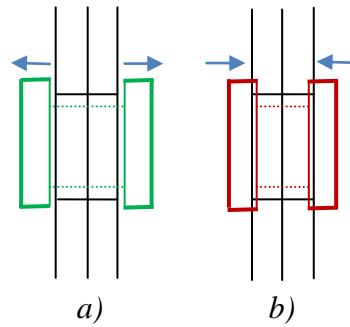
Figure 4.3*: Contact arrangement for bolt 1. a) Step 1 b) Step 2.*

Finally, another interaction to be considered in the FE model were the welds between the beam and the endplate. It was defined as a *Tie* constraint. For a structural analysis with ABAQUS this means that the translational and rotational degrees of freedom are constrained between the surfaces of the beam and the endplate which are in contact.

4.1.2. Mesh

Eight-node brick elements with reduced integration (C3D8R) were used for all parts in the model. Reduced-integration involves that the elements had just a single integration point located at the element's centroid. Applying Yu *et al*., 2008, the mesh was carefully symetrically defined on critical zones, such as the regions around the bolt holes where likely failures would initiate. Besides, for the contact between elements the meshing was done fine enough for each element's node of the master surface to face a corresponding node of the slave surface elements.

Figure 4.2 shows the meshing established for each part of the model. It can also be seen that for column and beams, different sizes of mesh were used. In order to obtain some simplification on the modelling, only fine mesh was defined when closer to the contact part of the model.
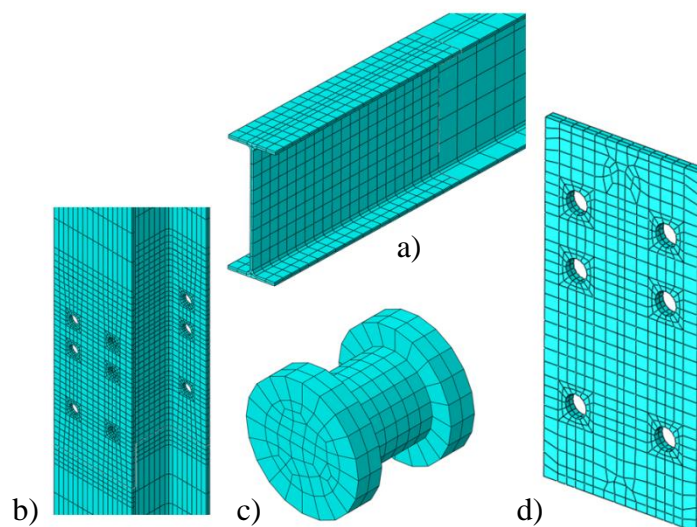
Figure 4.2*: Mesh pattern. a) beam, b) column, c) bolt, d) endplate.*

4.1.3. Boundary conditions

In order to prevent undesirable movements, the column had to be fixed at both top and bottom extremes during the whole simulation. This configuration was also established for the positioning conditions at the experimental tests. The column base was fixed using displacement restriction in every direction; while the upper part was restrained only in two directions, leaving free the vertical displacement.

The boundary conditions are quite crucial and have significant influence in modeling of the joint behaviour. To achieve sensible behaviour at the joint and move away from any singularity problems that may arise; each bolt is renstrained during the steps where the contact is established and then freed for later steps. The bolts restraint is defined at the nuts outer surfaces for displacement in every direction. Besides, to be more conservative during the contact process the beams were also restrained at their extremes during these first contact steps, and freed afterwards. Figure 4.3 shows these boundary conditions which concerns the contact interaction process.
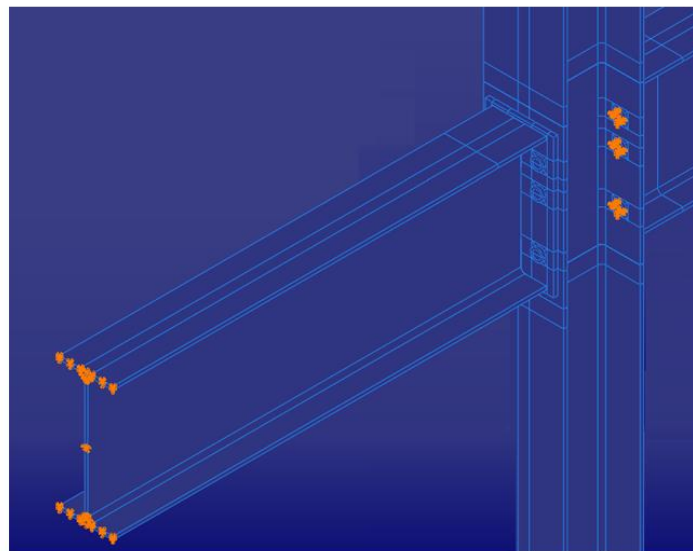
Figure 4.3: Boundary conditions applied for contact interaction process.

As can be noticed from the explanation above, the FE model boundary conditions vary during the complete analysis. At the beginning of the analysis everything is fixed. This means column at both top and bottom sides, beam extremes and bolts. These conditions last the whole contact process defined on 4.1.1, and when the last bolt contact is established two new steps are defined for the establishment of the ultimate boundary conditions. On the first step beams are released, and then bolts. The final boundary conditions maintained are the column restrictions. Only then the loading can be applied.

4.1.4. Load

Imitating the experimental tests load conditions, two concentrated loads were applied at the extreme of the beams at a distances of 1415,8 mm from the face of the column flange. For the ambient temperature model, the loading applied was 25 kN per beam. This makes a moment value at the joint of 35,4 kNm, which is over the design moment resistance obtained according to the Component Method results in chapter 3. The objective of this conditions is to analyse the behaviour of the joint up to the failure.

The joint tests used bolts tightened to a moment of 160 Nm. In ABAQUS, bolt pretension can be defined as a *bolt load*, so the relationship between moment and force on tightened bolts was necessary. In order to asses the magnitude of the force, expression 4.1 was applied (Airila, 2003).

$$F_M = \frac{2M_A}{1,155\,\mu_G d_2 + \mu_K D_{km} + \frac{P}{\pi}} \tag{4.1}$$

where

M_A is the bolt installation torque, $\qquad\qquad\qquad M_A = 160$ Nm

μ_G is the coefficient of friction of screw thread, $\qquad \mu_G = 0,2$

μ_K is the coefficient of screw (nut) surfaces, $\qquad\quad \mu_K = 0,2$

d_2 is the edge diameter, $\qquad\qquad\qquad\qquad\qquad d_2 = 30$ mm

P is the bolt pintch, $\qquad\qquad\qquad\qquad\qquad\quad P = 2$mm

D_{km} is the mean screw diameter, which is obtained from expression 4.2

$$D_{km} = \frac{d_k + D_B}{2} \tag{4.2}$$

where

d_k is the inside diametre of the conctact surface (washer inside diameter),

$$d_k = 18 \text{ mm}$$

D_B is the outside diameter of the contact surface (bolt head outside diameter),

$$D_B = 24 \text{ mm}$$

The value for pretension bolt load F_M, obtained from 4.2 was 27,2 kN.

4.1.5. Mechanical properties

Since ABAQUS is able to conduct large-deformation analysis, the elastic and plastic properties of the materials are needed to be defined. The material properties used on the joint model were determined from those used at the experimental results. The steel for all constructive elements but bolts was defined as steel Grade 43, and bolts were defined Grade 8.8. The effective material properties of the joint parts are summarized in Table 4.2.

Table 4.2: *Effective material properties*

	Young's modulus [kN/mm^2]	Poisson's ratio	Yield strength [N/mm^2]	Ultimate tensile strength [N/mm^2]
Steel	197	0,3	322	454
Bolts	210	0,3	640	800

The mechanical properties for both materials at ambient temperature were defined using the stress-strain relationship obtained from Eurocode 3, Part 1-2. These relationships are shown in Figure 4.4.
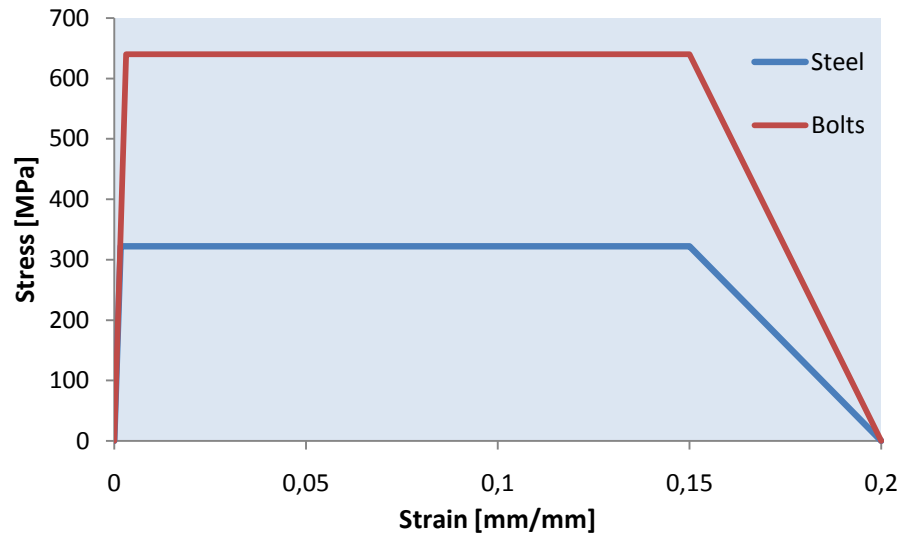
Figure 4.4: *Stress-strain relationship used to define the material properties for steel and bolts on FE model at ambient temperature.*

When defining plasticity data in ABAQUS, *true stress* and *true strain* values are required for a correct interpretation of the input file. The relationships between the nominal and true values are given on expressions 4.3 and 4.4

$$\sigma_{true} = \sigma\,(1+\varepsilon) \tag{4.3}$$

$$\varepsilon_{pl,true} = ln(1+\varepsilon) - \frac{\sigma_{true}}{E} \tag{4.4}$$

where

σ_{true} is the true stress,

σ is the nominal stress,

$\varepsilon_{pl,true}$ is the true plastic strain,

ε is is the nominal strain,

E is the Young's modulus.

As a simplification of the FE model the properties were only defined until the limiting strain for yield strength (15 % strain). This means that ultimate part of the behaviour-curve representing the steel fracture was not defined. However, failure was considered during the analysis by registering the equivalent plastic strain on ABAQUS model, and locating where was first reached 20% strain at the joint. Theodorou *et al*., 2001 was also used for maximum strain of bolts at elevated temperatures.

4.2. Results and Verification of FE Model against EN Calculations at Ambient Temperature

Since no experimental data were available for the studied case at ambient conditions, the initial validation of the model for ambient temperature was carried out using the results obtained from the spring-stiffness model, based on the Component Method. The comparison of the joint response is represented by the moment-rotation characteristic shown in Figure 4.5 until 80mrad, when ABAQUS model reached 33kNm. The rotation of each beam on the FE model was calculated using the approximation 4.5.

$$\varphi \sim \tan \varphi \;=\; \frac{(u_1 - u_2)}{h_b} \tag{4.5}$$

where

φ is the rotation,

u_1 is the displacement of the beam flange in tension (upper flange),

u_2 is the displacement of the beam flange in compression (bottom flange),
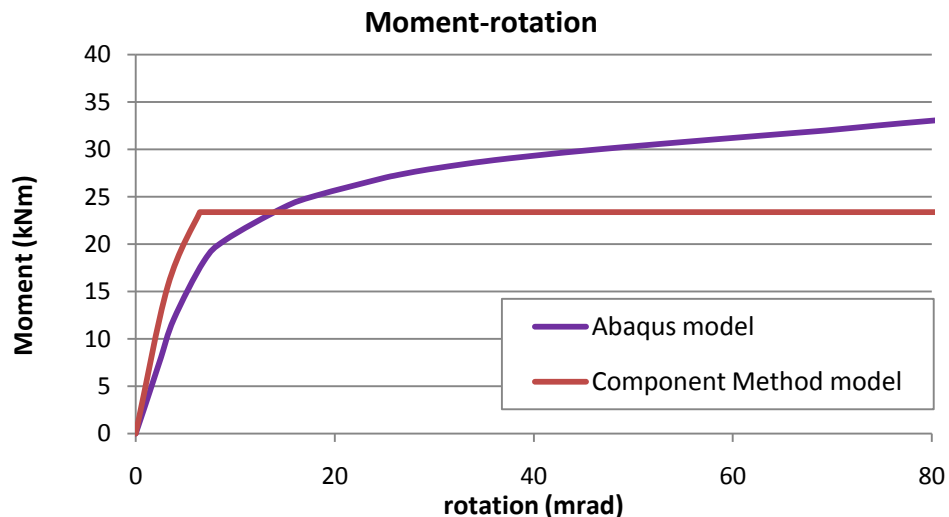
h_b is the beam height.

Figure 4.5: *Comparison of ambient temperature response of ABAQUS model with Component Method results.*

The joint behaviour obtained from the Finite Element model has an acceptable agreement with the proposed analytical method since both curves demonstrate a good correlation. The initial stiffness and strain hardening stiffness of the joint is closely represented, as well as the asymptotic tendency afterwards. However, as both cases represent analytical models the moment-rotation characteristic is not well described for the ultimate state. The Component Method only represents the first stage response of the joint, and after the moment resistance is reached (23,38kNm), it is maintained constant with no limiting rotation. On the other hand, ABAQUS analysis was full accomplished with a moment 35,4kNm obtaining a maximum rotation of 107mrad, which was not considered representative. The main reason was because of the material properties approximations taken for the model. As no failure properties are defined, the properties allow larger deformations.

The joint is shown in deformation state in Figure 4.6. The fracture strain criterion, represented by 20% plastic strain was not reached in any part of the model with this loading arrangement; however, the appearance of large deformation on the column flanges could be considered signal of failure. The maximum strain registered at the model was 15,45% and took place at the level of the first bolt row on the column flange as shows Figure 4.6 b. This gives a good concordance with the predicting failure mode of the joint according to the Component Method, which assessed the limiting component at the first bolt row for column flange in bending. The maximum strain considered for grade 8.8 bolts in ambient temperature is of order 5,2% (Theodorou, 2001). For this case, bolts did not experience big distortion.

<div align="center">a)   b)</div>
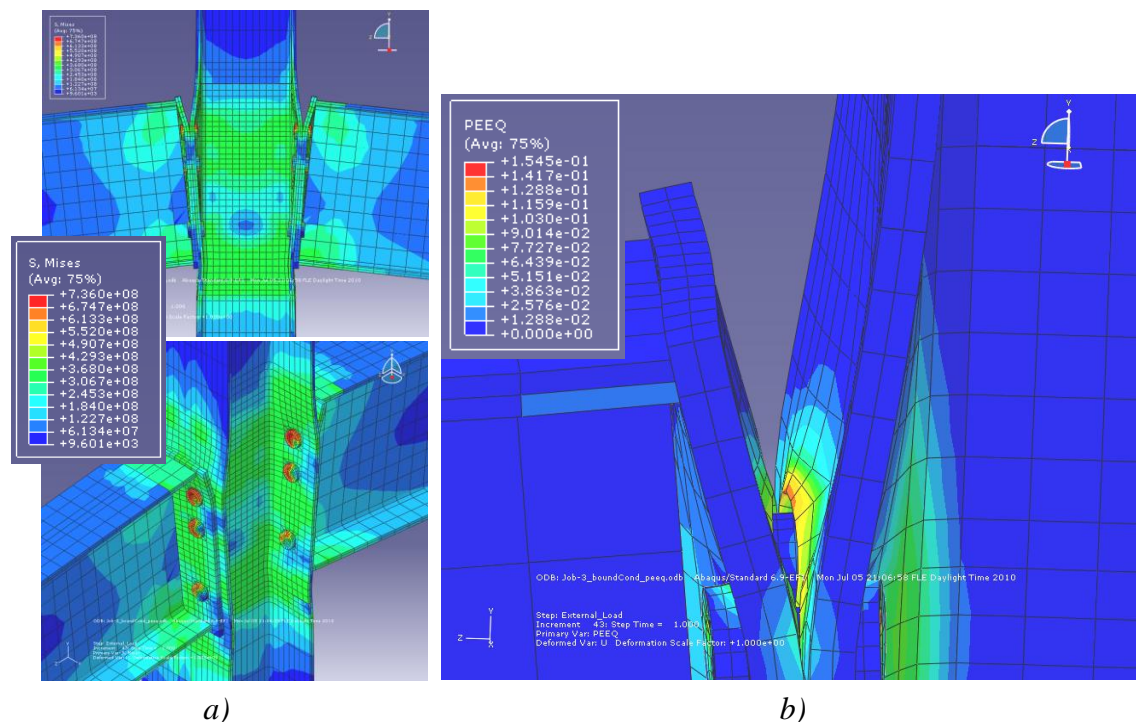
Figure 4.6*: Deformation of the beam-to-column model and the column flange with 35,4kNm moment. (a) Von Mises stress; (b) Equivalent plastic strain.*

As it was expected from the component model, the three bolt rows were subjected to tension. The maximum stress values registered for the model appeared on the bolt heads located on the first row. Von Mises stresses at bolts heads were 736MPa. On Figure 4.7 the maximum stresses are shown on the red coloured of the mesh. The deformation of the column flange in the tension zone and the buckling of the column web in the compression zone can also be seen on Figure 4.7.
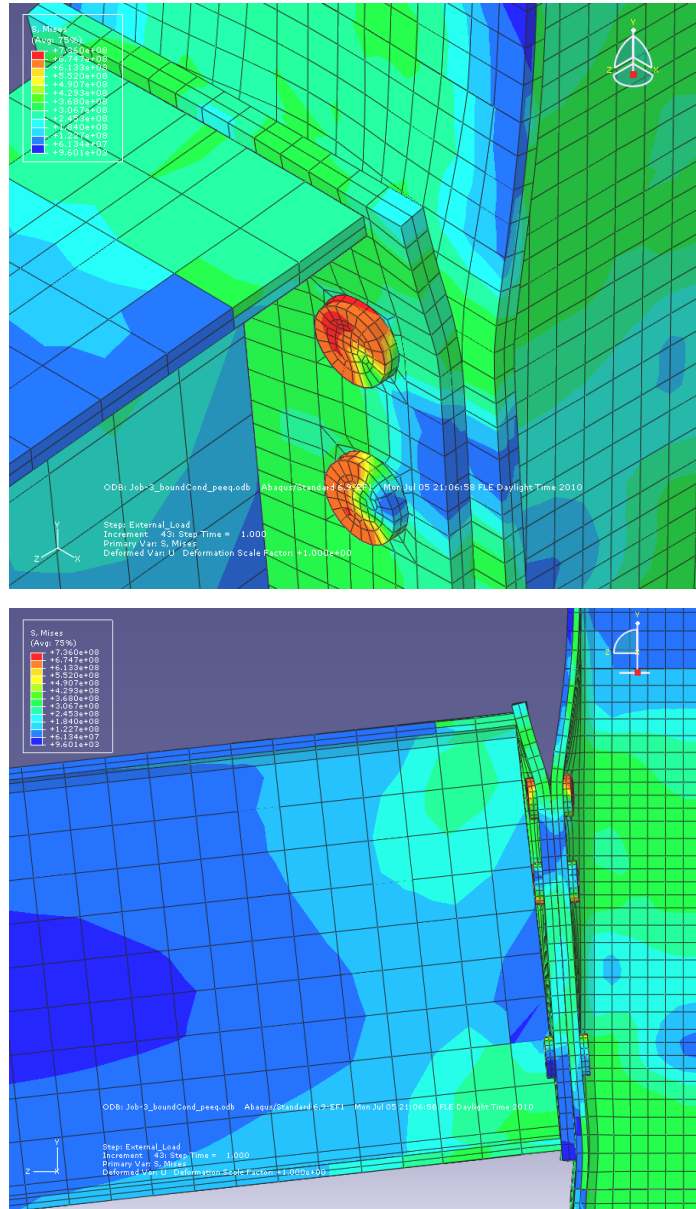
Figure 4.7*: Deformation of the beam-to-column model with 35,4kNm moment. Von Mises stress visualization.*

5. TEMPERATURE ANALYSIS

5.1. Finite Element Model with Temperature

The Finite Element model created to analyse the joint at ambient temperature was developed further to study the joint at elevated temperature. The simulations carried out were defined following the conditions of the experimental tests performed in Al- Jabri *et al.,* 1999. Some specifications about the test arrangements are detailed next.

5.1.1. Experimental test arrangements

The tests were conducted for a PhD Thesis at University of Sheffield for the investigation of the influence of connections characteristics on frame behaviour at elevated temperatures. Several test specimens were kept at a constant load level while increasing the furnace temperature until failure. The heating adopted was linear increase of temperature of 10ºC/min until 900ºC.

For the joint case which concerns this study, the column was firmly fixed in place at the base, and the top was secured in position but left free to move vertically. Similarly, the beams were only permitted to deflect downwards. Lateral movements, associated with possible buckling of the beams and which would result in premature termination of the test, were prevented by means of horizontal restraint. Fire protection was adopted for a large number of elements, and only the joint, column and beam sections within approximately 100 mm of the face of the joints were left exposed.

Three groups of tests on steel flush endplate joints were performed. The joint configuration for the Finite Element model was the same as for Group 1. Four different tests were conducted according to the loading conditions using the naming FB11, FB12, FB13 and FB14. The moment applied at the joint was approximately 4kNm, 8kNm, 13kNm and 17kNm respectively.

The instrumentation used to determine the elevated temperature characteristics of the joints included clinometers, displacement transducers and thermocouples. The rotational movement was measured using clinometers attached to each beam in line with the centre line; as well as several displacement transducers attached along the beam. The joint temperature and the thermal gradient across the section were monitored by thermocouples also located on the beams.

5.1.2. Model description

The joint model in fire conditions was created using the FE model at ambient temperature. The contact interaction stayed with the same arrangements, as well as the mesh definition. The starting steps where contact is established and boundary conditions fix every component, is maintained. Then beams and bolts are freed as happened at ambient temperature. Concentrated forces at the extremes of the beams were applied, and different simulations were performed varying the loading values according to the experimental tests; applying 2,8kN, 5,6kN, 9,2kN, 12kN respectively.

After applying the structural load the high temperature analysis was defined in several time steps. A uniform temperature distribution which increases during eight steps from 20 to 800 °C in a 100°C rate per step, creates the temperature increment at the joint. This action was only defined at the joint until 100 mm round from the beam flange. The rest of the structure was defined with temperature distribution of 20 °C. Figure 5.1 shows the nodal temperature that was registered along the structure during the analysis, according to this definition.
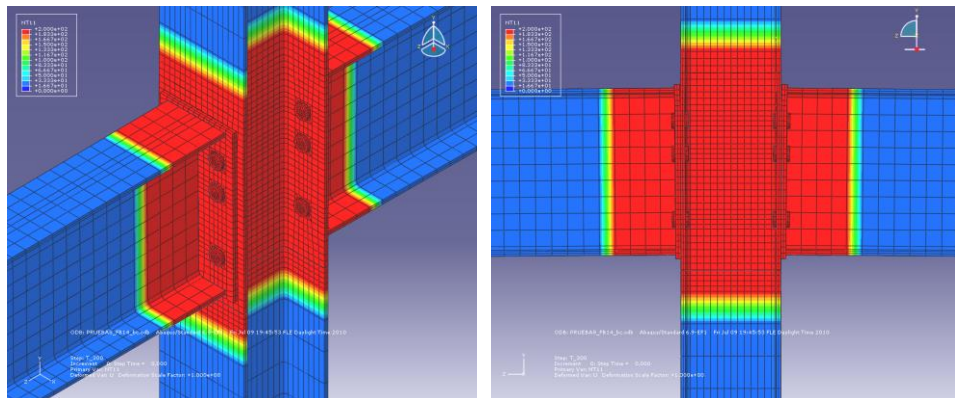
Figure 5.1*: Nodal temperature of the model during analysis.*

For this thermal analysis, the definition of the material properties at every temperature was needed. The mechanical properties for bolt and steel materials were defined at elevated temperatures using the stress-strain relationship obtained from Eurocode 3, Part 1-2. These relationships for both materials are shown in Figure 5.2. Poisson's ratio of steel at elevated temperatures was taken to be the same as at ambient temperature (ν = 0,3), and Young's modulus was defined using the reductions factors from EN 1993-1-2, 2005.
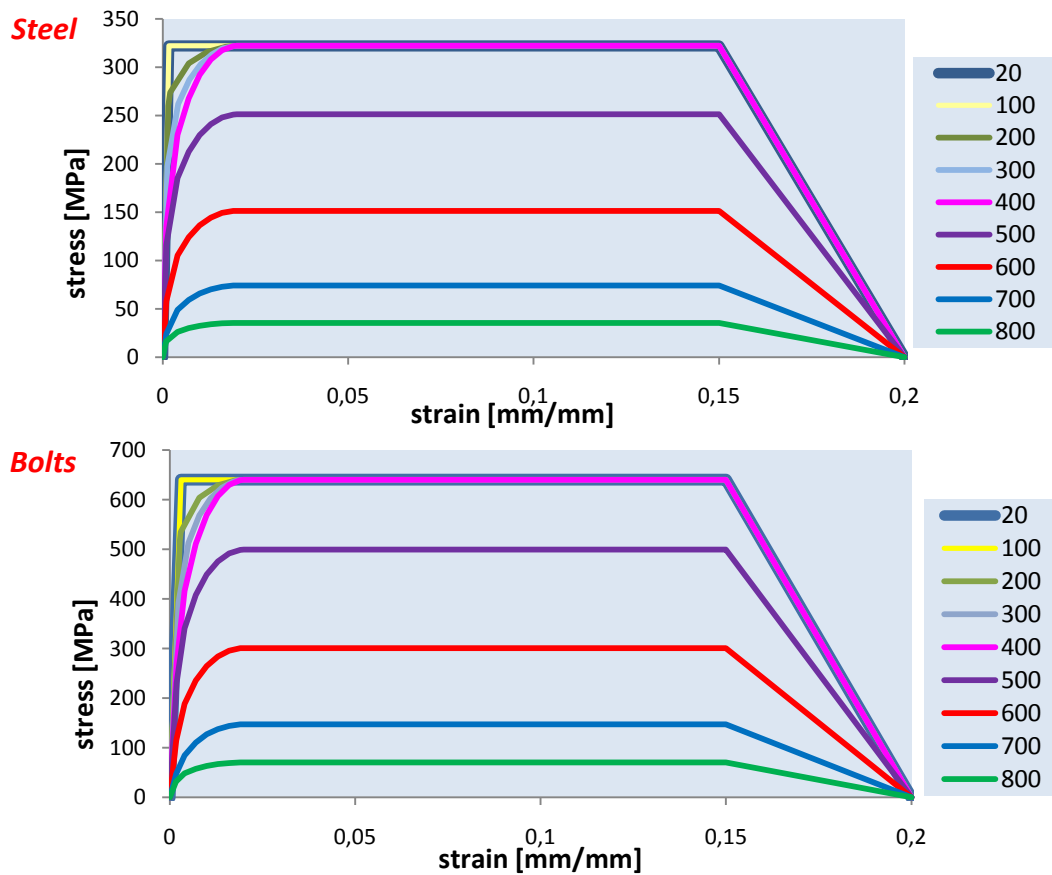
Figure 5.2*: Stress-strain relationship at elevated temperatures for steel and bolts.*

Moreover, the material properties of the model also included the thermal expansion of steel. The thermal expansion values at elevated temperatures were defined applying Eurocode 3. They were determined from thermal elongation at elevated temperature defined from codes using the relationship 5.1

$$\varepsilon_\theta = \alpha \, \Delta\theta \tag{5.1}$$

where

ε_θ is the relative thermal elongation,

α is the thermal expansion coefficient,

$\Delta\theta$ is the steel temperature [°C].

The values obtained and also introduced at the model are shown on Table 5.1.

Table 5.1*: Thermal expansion at elevated temperatures.*

$\Delta\vartheta$[°C]	20	100	200	300	400	500	600	700	800
ε_ϑ x10^{-3}	0,00	1,00	2,32	3,72	5,20	6,76	8,40	10,12	11,00
α x 10^{-6}	12,0	12,0	12,9	13,3	13,7	14,1	14,5	14,9	14,1

5.2. Results and Verification of Finite Element Model against Test Results

The model results obtained were compared against the temperature-rotation behaviour of the experimental tests. The validation of the model against the test results is shown from Figures 5.2 to 5.6. An average of the rotation on the beams is used in tests and FE model for the comparison.

5.2.1. Test FB11. Group 1, Fire test 1

The load applied at the beams was 2,8 kN, with a relatively low effect at the joint of approximately 4 kNm. Figure 5.3 shows the temperature-rotation behaviour in comparison with test results. The Finite Element model gives a good prediction of the initial deformation under the linear response. At higher temperatures the FE simulation seems to provide more resistance than tests.

As a result of the low loading of this case, the deformation and stresses suffered by the joint was not of great value as shown on Figure 5.3. The joint was capable of resisting temperature up to 575°C without experiencing any significant rotation. The deformation is approximately linear until 575°C, and from this temperature the rate of rotation increases due to yielding. The main differences between model and tests appear beyond this temperature. At temperatures exceeding 700°C the joint approaches failure on tests and the curve experiences a rapid increase of rotation, while FE model stays with the same rate. The model reaches 800°C with a rotation of 41mrad and the test joint fails around 750°C at a rotation of 60mrad.
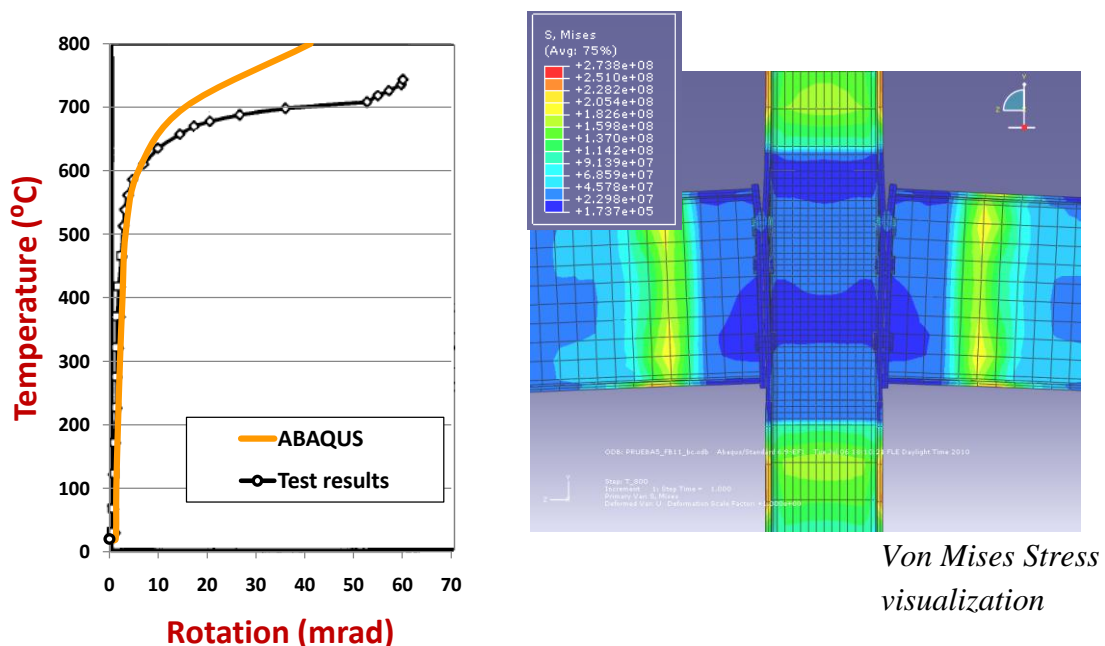

Von Mises Stress visualization

Figure 5.3*: FB11 (test 1). Comparison Temperature-Rotation characteristic and deformation state of the FE model.*

5.2.2.   Test FB12. Group 1, Fire test 2

For this simulation the loading was increased and the moment applied at the joint was approximately 8kNm. Figure 5.4 shows the comparison between FE model and test results. The behaviour of the curves shows that the deformation of the joint is followed by the numerical model. In this case the simulation results are more accurate, and even when steel enters the state of plastification the response is close to test results. The joint fails around 80mrad on tests, while the model continues deforming. Figure 5.4 shows the remarkable deformation of the joint when the analysis is completed. The plastic strain is observed to overpass 20% before the full analysis is accomplished. This strain criterion proposed, defines the model failure at the shank of the bolts located on the first row at a temperature of 757°C and a rotation of 128mrad. Figure 5.5 shows the bolts deformed at full analysis.
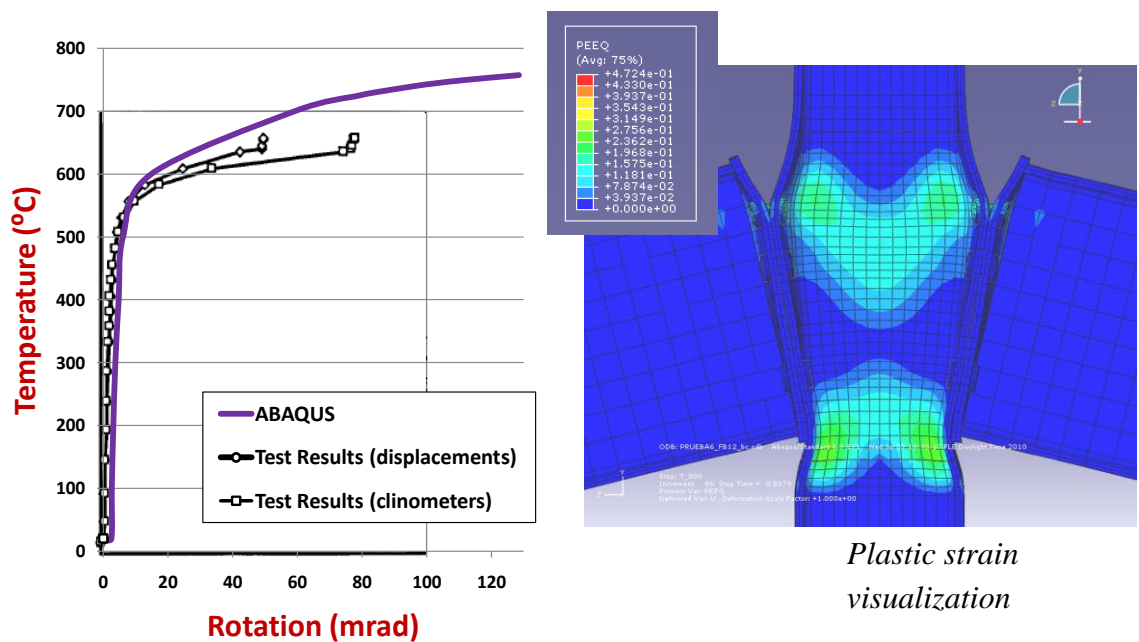

Plastic strain visualization

Figure 5.4*: FB12 (test2). Comparison Temperature-Rotation characteristic and deformation state of the FE model.*
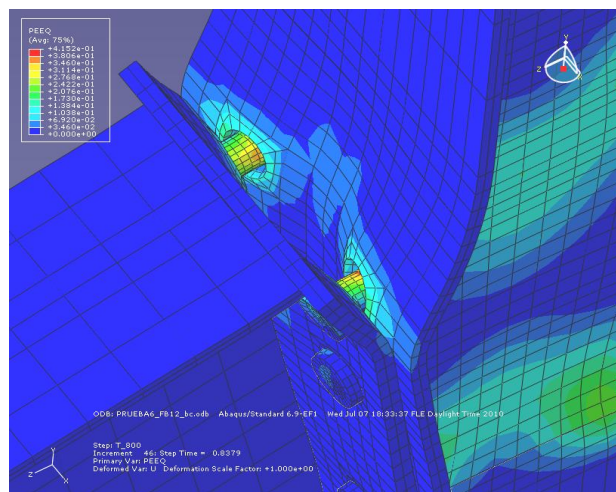

Figure 5.5: *Plastic strain and deformation at the first bolt row.*
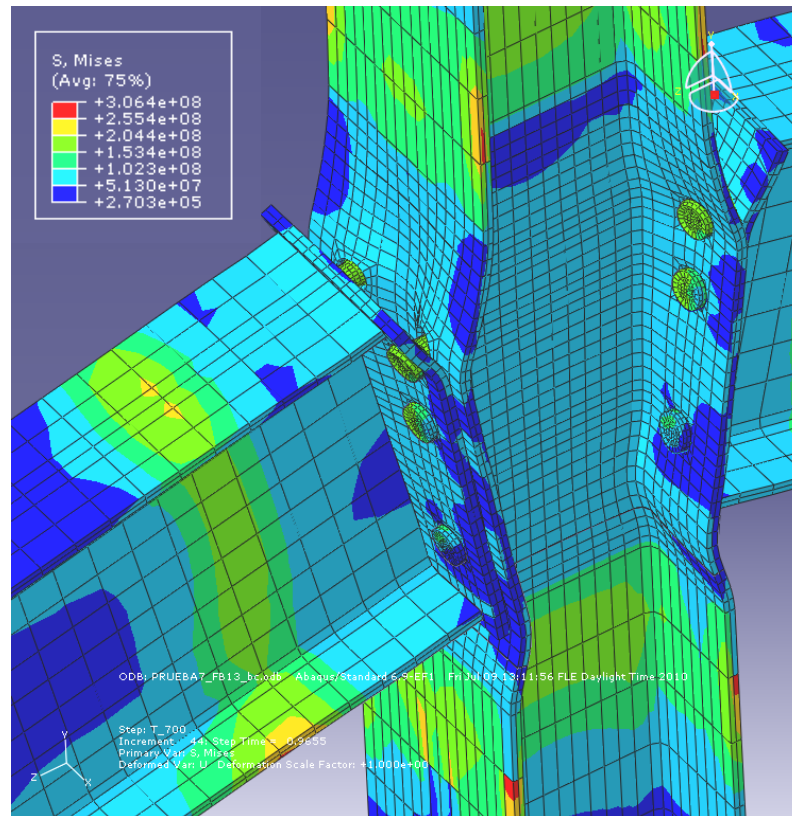
5.2.3. Test FB13. Group 1, Fire test 3

Next two simulations were increased on the loading arrangement giving results more representative for analysis. The moment applied at the joint on fire test 3 was 13kNm. Figure 5.6 shows the comparison between Finite Element model and test results. As happened on previous cases the joint deforms in a good concordance with tests. Around 550°C the rotation increases rapidly due to yielding, and during the plastification state both curves behave similarly. Plastic strain was registered during the analysis and shank bolts experienced the highest distortions. 5% strain appeared first on the model at 640°C, 10% at 656°C, 15% at 668°C and the fracture strain supposed at 20% plastic strain was registered at the bolt when the model reached 675°C with a rotation on the joint of 136,87mrad. Considering grade 8.8 bolts maximum strain at elevated temperatures (Theodorou, 2001), the FE model might fail around 660°C with 16% strain.
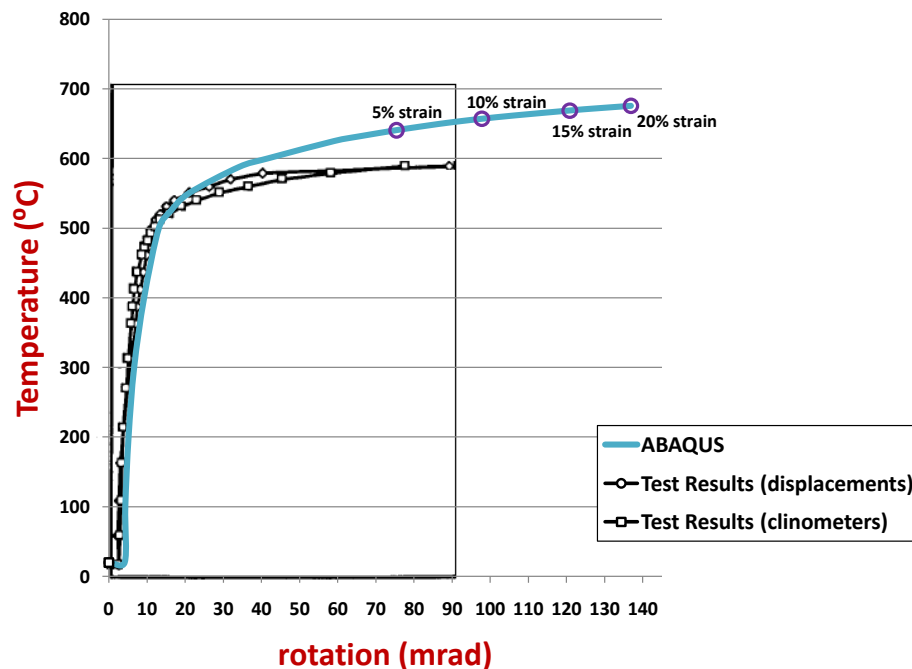
Figure 5.6*: FB13 (test 3). Comparison Temperature-Rotation characteristic.*

Apart from bolt shank strains, large deformations were also considered when searching for failure approaches. Column flange and endplate were observed to deform considerably, especially at the level of the first bolt as shows Figure 5.7. Particularly, taking into account the weld joining endplate and beam on real case, a possible failure mechanism due to rupture of the weld is also considered. Besides, the compression zones of the joint have large deformations at the column flanges.

Figure 5.7: *Deformation of the joint after full analysis. Column flange and endplate at the first bolt row and column flange at the compression zone.*

5.2.4.   Test FB14. Group 1, Fire test 4

The last simulation was performed applying a moment at the joint of 17 kNm. Figure 5.8 shows the comparison of the temperature-rotation behaviour between FE model and test results. The model and test results show a close deformation against temperature. Since remarkable limiting conditions are achieved due to the high loading of the case, the results are more interesting for analysis. The FE model registered maximum plastic strain values during the simulation at the bolt shanks of the first row. 5% strain was reached at 590°C, 10% at 612°C, 15% at 622°C and 20% fracture strain was reached at 638°C with 155mrad rotation. Using Theodorou *et al*., 2001, grade 8.8 bolts fail at 600 °C with a plastic strain around 9% and 92mrad rotation.

The deformation accomplished by the joint was similar to previous case, and excessive distortion was observed for column flange at both tension and compression zone, as well as for endplate at the upper part until the level of first bolt row (Figure 5.9). The release of stresses at the joint is known as a common conduct on fire. Due to the larger loading conditions this behaviour was demonstrated more clearly during this simulation. Figure 5.9 shows Von Mises stresses average registered on the nodes of the column flange at the level of the first bolt holes and on the bolt heads in comparison with the temperature.
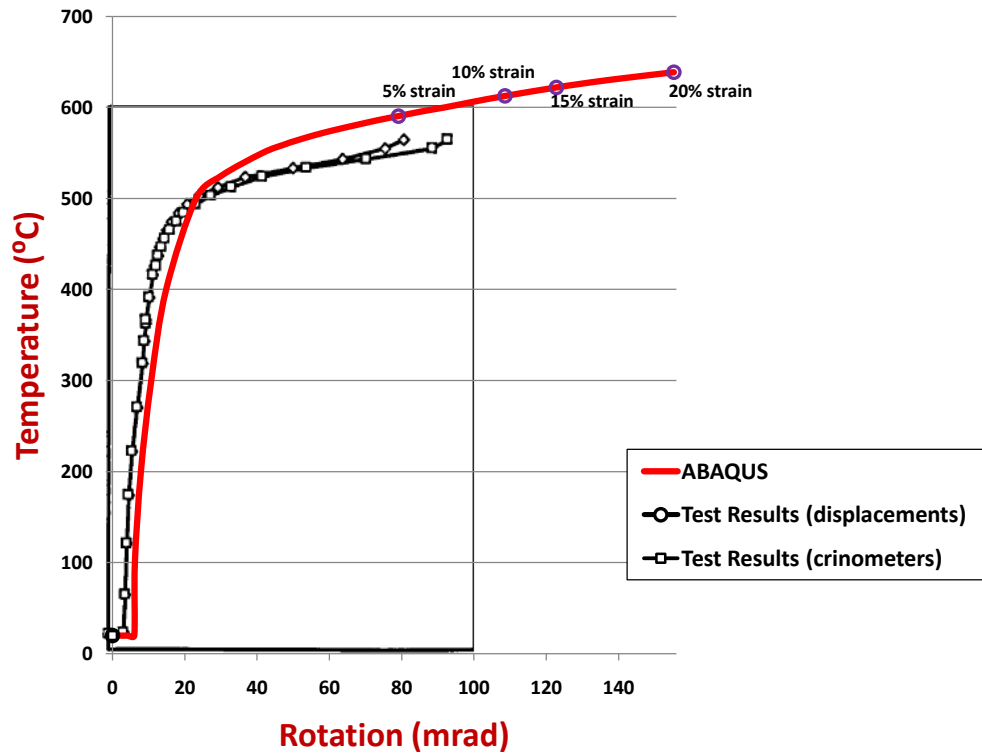
Figure 5.7: *FB14 (test 4). Comparison Temperature-Rotation.*
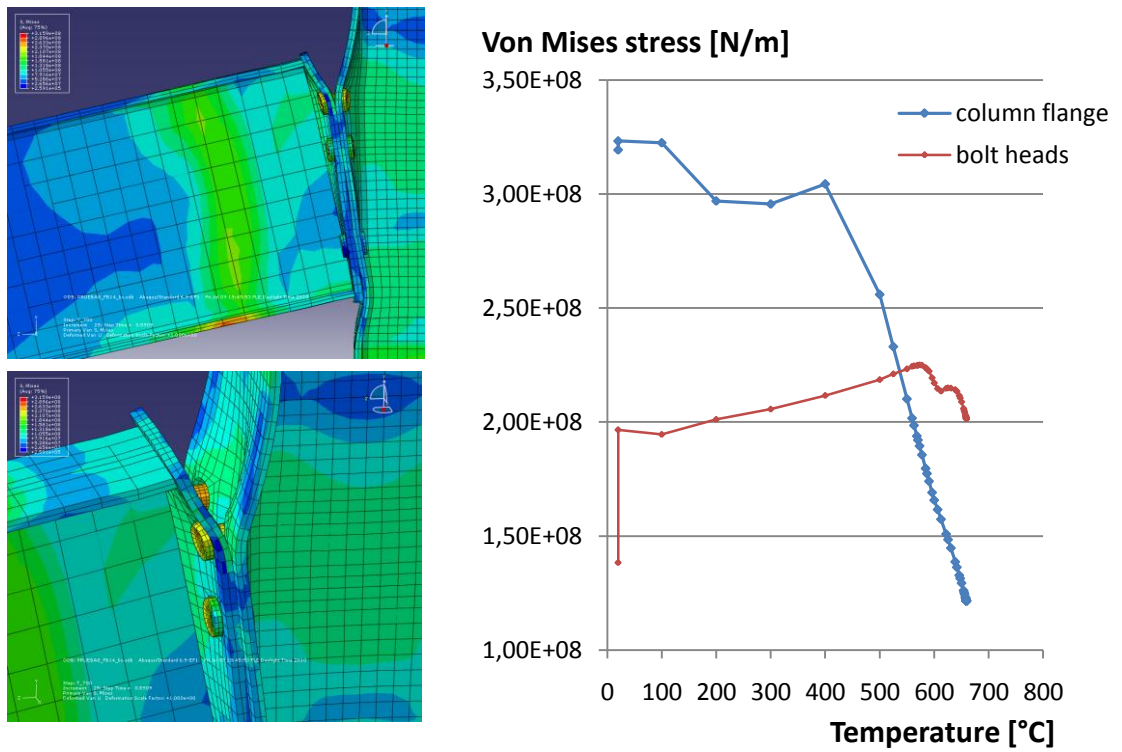

Figure 5.9: *Release of stresses for the column flange and bolt heads during the analysis.*

5.2.5. General observations and conclusions

The definition of steel properties without including fracture strain made difficult to evaluate the model when approaching to failure; however, in all cases the FE model has proved satisfactory results when comparing with test results.

Al Jabri, *et al*., 1999 described the modes of failure in all tests conducted to be similar in that the endplate deformed locally, particularly around the top bolt. This was accompanied by deformation of the column flange in the tension zone and buckling of the column web in the compression zone as shown on Figure 5.10. All these behaviours agree with the failure predicted for the model on previous sections. Besides, there was negligible deformation of the beams along their entire length, as happened on the finite element model. On the tests it was also observed no distortion of the bolts and no sign of slip at the joint interface, demonstrating the efficiency of the bolts in resisting the applied tension forces and moments. For the FE model great distortion was established at the bolts, which defines disagreement with test results. The deformation of the patterns obtained by simulation and from the tests is very close as shown on Figure 5.10.
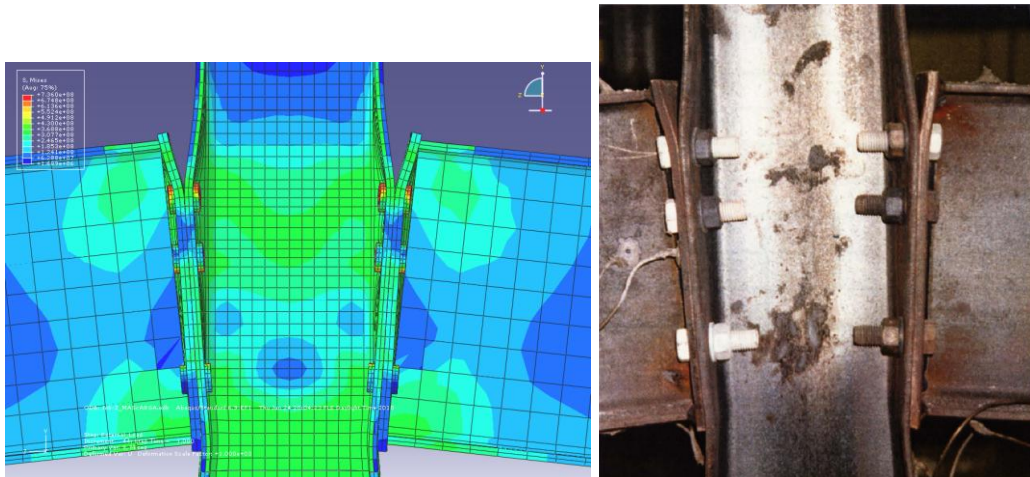
Figure 5.10: *Comparison of observed deformation on simulation and tests.*

5.3. Component Method at Elevated Temperatures

During the second chapter the Component Method was used to model the joint and predict the joint's response by assembling the stiffnesses of the components. The structural properties were represented by the Design Moment Resistance and the Rotational Stiffness. At elevated temperature steel is assumed to degrade, and the structural properties can be reduced with increasing temperatures based on the recommendations presented in the standards. For the case of study it was taken into consideration the bolted joint as a representative agent, and the Design Moment Resistance was reduced using the strength reduction factors for bolts, $k_{b,\theta}$, which are

meant for bolts and bearing strengths in the joints. The reduction factors for yield strength, $k_{f,\theta}$ are also recommended on standards for steel elements, and for this case they were also considered to reduce the Design Moment Resistance in order to analyze and compare the effect of both ways of reduction. The Rotational Stiffness was reduced with temperature by Young's modulus reduction factors, $k_{E,\theta}$. Table 5.2 shows the values for reduction factors on structural steel at elevated temperatures. The application of these reduction factors give the values shown on Table 5.3, which result on a representation of the moment-rotation characteristic for the studied case at elevated temperatures as shows Figure 5.11.

***Table 5.2****: Properties of structural steel at elevated temperatures (EN 1993-1-2, 2005).*

Temperature [°C]	$k_{b,\theta}$ reduction factor for Design Moment Resistance	$k_{f,\theta}$ reduction factor for Design Moment Resistance	$k_{E,\theta}$ reduction factor for Rotational Stiffness
20	1	1,000	1
100	0,968	1,000	1
200	0,935	1,000	0,9
300	0,903	1,000	0,8
400	0,775	1,000	0,7
500	0,55	0,780	0,6
600	0,22	0,470	0,31
700	0,1	0,230	0,13

Table 5.3 a*: Representative values for defining the moment-rotation characteristic of the joint at elevated temperatures at initial state.*

Temperature [°C]	$S_{j,ini}$ [kNm/rad]	$\frac{2}{3} M_{j,Rd}$[kNm]		$\varphi_{X,ini}$ [mrad]	
		$k_{b,\theta}$ red. factor	$k_{f,\theta}$ red. factor	$k_{b,\theta}$ red. factor	$k_{f,\theta}$ red. factor
20	4841,98	15,59	15,58	3,22	3,22
100	4841,98	15,09	15,58	3,12	3,22
200	4357,78	14,57	15,58	3,34	3,57
300	3873,58	14,07	15,58	3,63	4,02
400	3389,38	12,08	15,58	3,56	4,60
500	2905,19	8,57	12,15	2,95	4,18
600	1501,01	3,43	7,32	2,28	4,88
700	629,46	1,56	3,58	2,47	5,69

Table 5.3 b: *Representative values for defining the moment-rotation characteristic of the joint at elevated temperatures.*

Temperature [°C]	S_j [kNm/rad]	$M_{j,Rd}$[kNm]		φ_X [mrad]	
		$k_{b,\theta}$ red. factor	$k_{f,\theta}$ red. factor	$k_{b,\theta}$ red. factor	$k_{f,\theta}$ red. factor
20	2420,99	23,38	23,38	6,44	6,44
100	2420,99	22,63	23,38	6,23	6,44
200	2178,89	21,86	23,38	6,69	7,15
300	1936,79	21,11	23,38	7,27	8,05
400	1694,69	18,12	23,38	7,13	9,20
500	1452,59	12,86	18,23	5,90	8,37
600	750,5	5,14	10,99	4,57	9,756
700	314,72	2,34	5,38	4,95	11,39
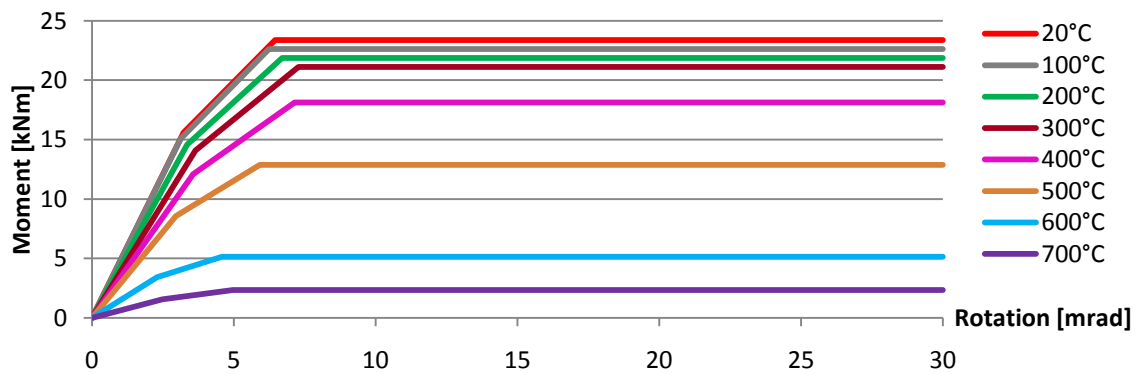
Figure 5.11a: *Moment-rotation characteristic at elevated temperatures using the Component Method, with $k_{b,\theta}$ reduction factor.*
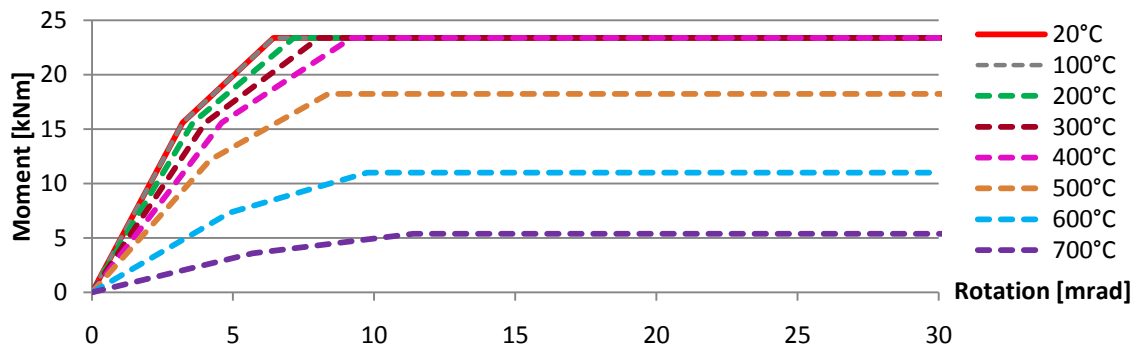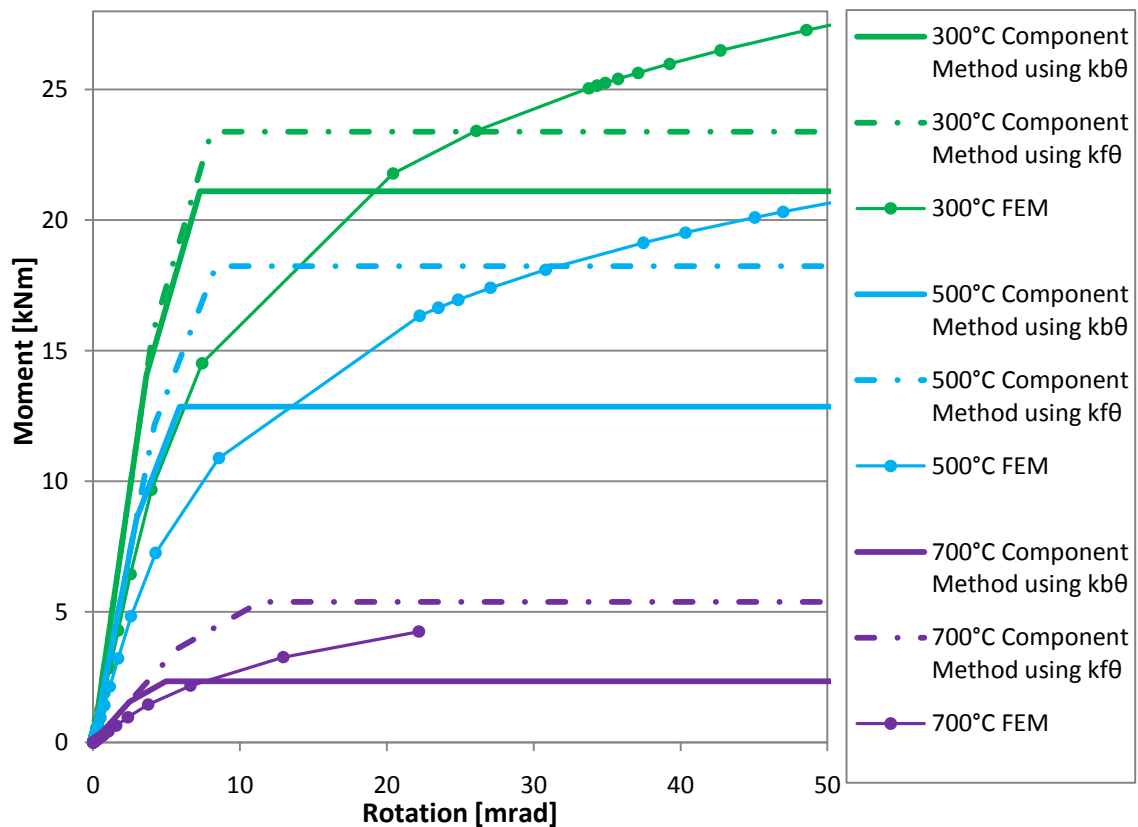

Figure 5.11b: *Moment-rotation characteristic at elevated temperatures using the Component Method, with $k_{f,\theta}$ reduction factor.*

It can be observed from the values above and Figure 5.11 that the main difference between using reduction factors for bolts and yield strength at the Component Method, is on the moment resistance. Using the bolts reduction factors the joint behavior obtained is more conservative, since they established smaller Design Moment Resistances than those obtained with the reduction factors for yield strength. On the other hand, the initial deformation under the linear response does not show difference between both cases.

5.4.   Comparison between Component Method and Finite Element Model

The Finite Element model was also simulated at elevated temperatures for validation against the Component Method model. In this case the model was defined using the same arrangements as the ambient conditions model. No thermal distribution was considered nor temperature increase. Instead, the material properties were defined according to the stress-strain relationship at the temperature which was going to be compared with. Three simulations were performed at 300°C, 500°C and 700°C respectively, using the material properties of steel and bolts for these temperatures. The loading was arranged taking into account the results obtained with the Component Method, ensuring representative moments at the joint on each case. For 300°C the moment applied at the joint was 28,3 kNm for 500°C was 21 kNm and for 700°C was 4,2kNm.

Figure 5.12 show the results obtained and the comparison of the moment-rotation characteristic between the FE model and Component Method. A good concordance between models is observed for the three simulations. During the initial deformation the Component Method gives in all cases more resistance than ABAQUS model, but still the behaviour stays very close between models. These comparisons at elevated temperatures add also validation to the FE model.

Figure 5.12: *Comparison of the moment-rotation characteristic temperatures between Component Method model and Finite Element model at 300°C, 500°C and 700°C.*

6. ANALYSIS WITH NEW LOADING CONDITIONS

The study which has been accomplished along the previous sections had the main objective of validating the Finite Element model created with ABAQUS for further research at both ambient and elevated temperatures. The satisfactory results obtained give the chance of extending the model by adding new loading conditions. Until now, the model has been subjected to vertical loading on the beams involving bending moment around the strong axis; which can be considered a close situation of a joint within a structure. The results could be compared against available experimental results as well as the component method since for this loading case it follows strictly the rules given in the standard. However, taking into account the loading distribution on steel framed structures; beams may also support horizontal loading and 3D bending at the joint becomes also interesting for study, especially for fire conditions. Along this chapter bending moment around the weak axis on the beam-to-column bolted joint is considered using the FEM model and the Component Method on 3D. For this case, tests results are not available.

6.1. Component Method Analysis Applied to 3D Loading

Standards only apply Component Method to planar joints, so extensions out of Eurocodes had to be considered for the new loading conditions. Heinisuo et al., 2009 proposed enlargement of the Component Method into 3D. The main idea is that the properties of the components given in the standards (EN 1993-1-8, 2005) are used as long as possible. When analyzing beam-to-column bolted joints in 3D, only the compression components differ from those given in the standard. The equations used in the analysis are the same but the differences are in the geometrical forms of the features.

A 3D loading arrangement with bending moment around the weak axis at the bolted joint is considered for this study, as shown on Figure 6.1 a. Only compression and tension components integrate the component analysis, excluding shear components. The beam section is divided into tension and compression zones. Bolt centers are the potential tension components, and one third of the beam flanges are the potential compression components (Figure 6.1 b). The tension resistances are for bolts in tension, column flange in bending and endplate in bending; and the compression resistance is due to beam flange in compression.
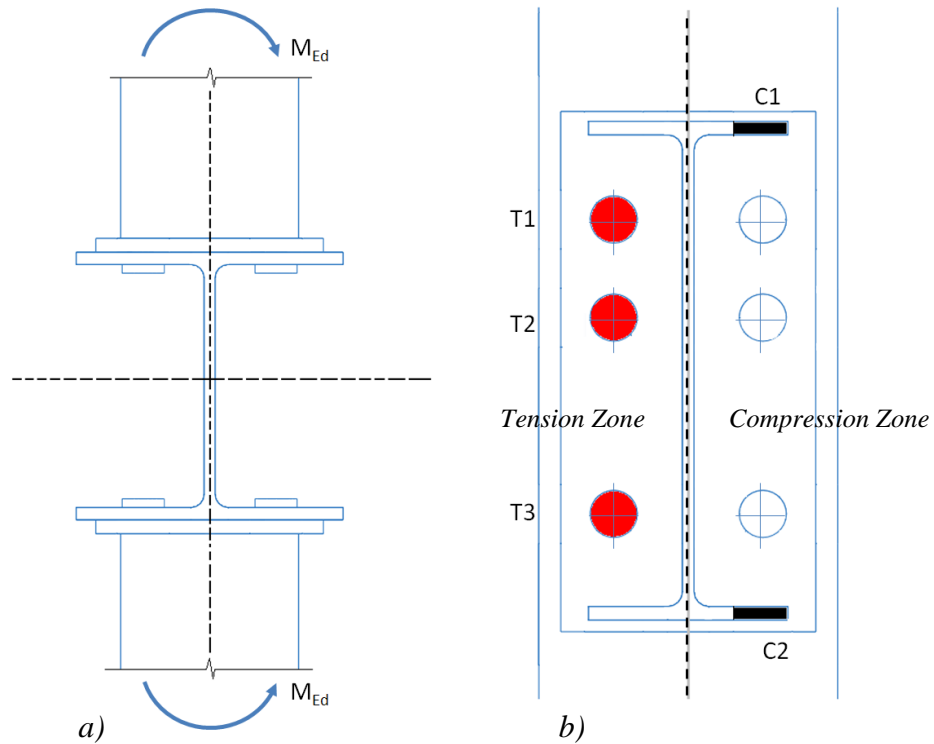
Figure 6.1*: a) Loading with bending moment around the weak axis. b) Potential tension components (T1, T2, T3) and potential compression components (C1, C2).*

6.1.1. Tension Design Resistances

The design tension resistance for the individual bolts is maintained the same as the magnitude assessed on chapter 3 for normal bending conditions (See 3.3.1). The value for the design resistance for bolts subjected to tension $F_{t,Rd}$, is 113 kN.

For column flange in bending, the design tension resistances and failure modes are determined from those of normal bending (See 3.3.2), but taking into account that the expressions given on Eurocodes consider two bolts per row. The components for bending around weak axis involve one bolt per row, so the values previously obtained have been divided by two. Table 6.1 summarize the results.

Table 6.1*: Tension resistances on each failure mode for column flange in bending.*

	$F_{T,1,Rd}$	$F_{T,2,Rd}$	$F_{T,3,Rd}$
Bolt row 1	42,1 kN	65,5 kN	113 kN
Bolt row 2	42,1 kN	65,5 kN	113 kN
Group bolt rows 1+2	55 kN	123,4 kN	226 kN
Bolt row 3	42,1 kN	65,5 kN	113 kN
Group bolt rows 2+3	67,9 kN	126,7 kN	226 kN
Group bolt rows 1+2+3	80,8 kN	184,7 kN	339,1 kN

The design tension resistances for column flange in bending for individual bolt rows and group of bolt rows are the minimum of the three mode values. In all cases corresponds to failure mode 1 (complete yielding of the flange) with noncircular patterns.

Finally, the last tension resistance considered is for endplate in bending. The values to be assigned for the design tension resistances and failure modes are obtained following the same consideration above. Values assessed on chapter 3 (See 3.34) have been divided by two, and Table 6.2 summarize the results. The design tension resistances for endplate in bending for individual bolt rows and group of bolt rows are the minimum of the three mode values. In all cases corresponds to failure mode 1 (complete yielding of the flange) with noncircular patterns.

Table 6.2: *Tension resistances on each failure mode for endplate in bending.*

	$F_{T,1,Rd}$	$F_{T,2,Rd}$	$F_{T,3,Rd}$
Bolt row 1	55,1 kN	67,6 kN	113 kN
Bolt row 2	52,6 kN	67 kN	113 kN
Group bolt rows 1+2	72 kN	129,3 kN	226 kN
Bolt row 3	54 kN	67,3kN	113 kN
Group bolt rows 2+3	87,8 kN	129,3 kN	226 kN
Group bolt rows 1+2+3	107,2 kN	187,5 kN	339,1 kN

6.1.2. Compression Design Resistance

The compression components for these loading conditions are one third of the beam flanges at the compression zone as it was previously said. The resultant of the design compression resistance of the beam flange may be assumed to act at the level of the centre of compression, which is located in the middle line of the extreme third part of the beam flange, as shows Figure 6.2.
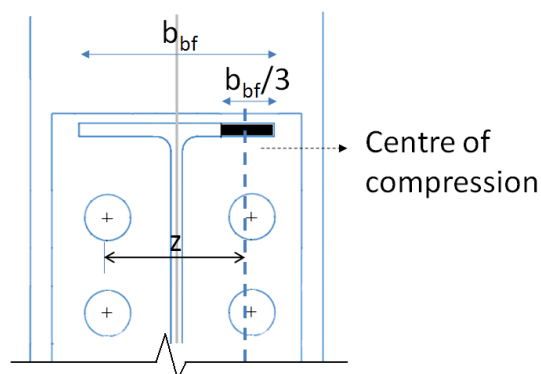
Figure 6.2: *Centre of compression at the beam flange with 3D loading conditions.*

The design compression resistance of the beam flange is given by the expression 6.1.

$$F_{c,fb,Rd} = \frac{M_{c,Rd}}{z}$$ (6.1)

where

z is the distance from the the bolts of the tension zone to the centre of compression, $z = 71,86$ mm

$M_{c,Rd}$ is the design moment resistance for bending of the beam cross-section. From EN 1993-1-1: 2005 it is determined with the equation 6.2.

$$M_{c,Rd} = M_{pl,Rd} = \frac{W_{pl} f_{yb}}{\gamma_{M0}}$$ (6.2)

where

W_{pl} is the plastic section modulus of the beam, $W_{pl} = 37,30$ cm^2

f_{yb} is the beam yield strength, $f_{yb} = 322$ N/mm^2

γ_{M0} is the partial safety factor for resistance of cross-sections, $\gamma_{M0} = 1,0$

The design moment resistance $M_{c,Rd}$, obtained from 6.2 is 12 KNm; and the design resistance for beam flange in compression $F_{c,fb,Rd}$, obtained from 6.1 is 167,1 KN.

6.1.3. Assembly of Components and Design Resistances

Table 6.3 shows the limiting component design resistances resultant to the case of study.

Table 6.3: Limiting components and design resistances.

Row	Component	F_{Rd}
1	Column flange in transverse bending	**42,1kN**
2	Column flange in transverse bending (group of bolt rows 1+2)	55-42,1 = **12,9kN**
3	Column flange in transverse bending (group of bolt rows 1+2+3)	80,8-42,1-12,9 = **25,8kN**

6.1.4. Structural properties

The Design Moment Resistance $M_{j,Rd}$, is determined from expression 6.3

$$M_{j,Rd} = z \sum F_{tr,Rd}$$ (6.3)

where

$M_{j,Rd}$ is The Design Moment Resistance

$F_{tr,Rd}$ is the effective design tension resistance of bolt-row r;

z is the distance from bolt-row r to the centre of compression; $z = 71,86$ mm

r is the bolt-row number.

The design moment resistance $M_{j,Rd}$, obtained from 6.3:

$$\boxed{M_{j,Rd} = 5,8\text{kNm}}$$

The Component Method is also able to introduce the presence of stiffeners on the calculations. It only affects the effective lengths of the column flange in bending and the final result of the moment resistance changes from 5,8 to **6,06kNm**, which involves not big difference.

The Rotational Stiffness is obtained using the same method as those used for bending moment around strong axis. The stiffness coefficients are assessed with the same equations, but only one bolt per row is considered and the values obtained have been divided by two (See 3.7.2). Table 6.4 summarize the stiffness coefficients obtained.

Table 6.4: Components and stiffness coefficients (effective coefficients and equivalent stiffness coefficients).

Component	Stiffness Coefficient		
	Bolt row 1	**Bolt row 2**	**Bolt row 3**
Column flange in bending	$k_{4,1}$=0,63mm	$k_{4,2}$=0,44mm	$k_{4,3}$=0,77mm
End plate in bending	$k_{5,1}$=0,89mm	$k_{5,2}$=0,6mm	$k_{5,3}$=1,07mm
Bolts in tension	$k_{10,1}$=4,77mm	$k_{10,2}$=4,77mm	$k_{10,3}$=4,77mm
$k_{\text{eff,r}} = \dfrac{1}{\Sigma_i \frac{1}{k_{i,r}}}$	$k_{\text{eff,1}}$=0,34	$k_{\text{eff,2}}$=0,24	$k_{\text{eff,3}}$=0,41
Equivalent	$\mathbf{k_{eq}} = \Sigma\, k_{eff,r} = \mathbf{0,99\ mm}$		

The Rotational Stiffness is obtained from equation 6.4

$$S_j = \frac{k_{eq} E\, z^2}{\eta} \tag{6.4}$$

where

|	
E is the Young's modulus,	$E = 197$ KN/mm^2
z is the lever arm,	$z = 71,86$ mm
η is the stiffness ratio $S_{j,ini}/S_j$	$\eta = 2$

The Rotational Stiffness S_j, and initial Rotational Stiffness $S_{j,ini}$, obtained from equation 6.4:

$$\boxed{S_j = 505,67\ \text{kNm/rad} \quad S_{j,ini} = 1011,34\ \text{kNm/rad}}$$

6.2.   Finite Element Model with ABAQUS

The same Finite Element model of previous simulations (See description on 4.1) was used to study the joint behavior with the new loading conditions. To establish 3D loading, the concentrated forces had to be modified. They were located on both beam extremes at the middle point of the web section, and changed from vertical to horizontal direction. Several analyses were carried out for this new study at ambient and elevated temperatures. The Component Method at 3D loading conditions developed on previous section was used to compare the results obtained at ambient conditions. The component model does not take into account the column web deformation, which originates some conflicts for the comparison. In order to achieve a suitable situation, ABAQUS model was extended by adding four 10mm thick stiffeners, as shown on Figure 6.3. The weld between stiffeners and column was simulated using *Tie* constraint.
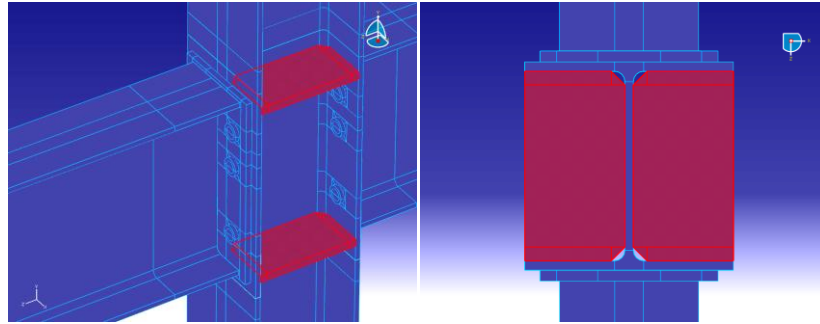
Figure 6.3*: FE model with four stiffeners of 10mm thickness.*

One simulation at ambient temperature and small loading was run for analysis leaving aside the stiffeners. Although it is not subject of this study, the behavior of the joint when deforming column web remains interesting, and adds information for possible further researches. Finally, temperature analysis was introduced to the model using transient tests with increasing temperature distribution (See model description on 5.1.2).

In order to study the deformation of the joint, the displacement of seven nodes at beam flanges was registered during the analyses, and the rotation of each flange was calculated using the approximation 6.5. An average of both beams flanges was considered for the global rotation.

$$\varphi \sim \tan \varphi \ = \ \frac{(u^*-u^{**})}{b} \tag{6.5}$$

where

φ is the rotation,

u^* is the displacement on the extreme node of the beam flange in the tension zone,

u^{**} is the displacement on the extreme node of the beam flange in the compression zone. When stiffeners are used the last node does not contribute to the rotation and the displacement is on reference of the second last node.

b is the distance between nodes. Without stiffeners it is equal to the width of the beam flange.

6.3.   Results at Ambient Temperature

Three different analyses were performed at ambient temperature; two of them using stiffeners and varying the loading conditions, and a third one without stiffeners and small load. The loading values were established applying moments at the joint close to the result obtained for the moment resistance with the Component Method. On the first analysis the load applied at the joint was a relatively small moment of 8,5kNm. On the second one, the moment was increased to 17kNm and the third analysis without stiffeners had a moment of 2,8kNm.

6.3.1.   Analysis 1

During the first simulation the model only experienced appreciable deformation on the beam flanges at the joint level, and on the endplate. Figure 6.4 shows the deformation of the model on the beam flanges, and presents the node displacements registered when the full analysis was accomplished (u_z values are expressed in meters, and come from the average of the displacements of the same nodes at both flanges). As it can be noticed, the joint did not experienced large deformations.
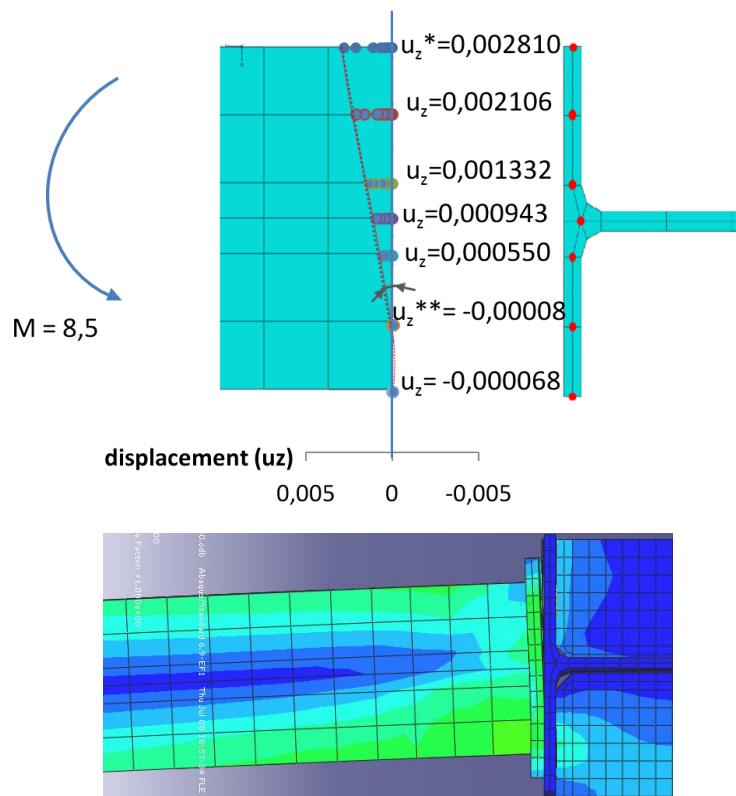

Figure 6.4: Beam flange displacement with 8,5kNm bending moment around weak axis.

When comparing the moment-rotation characteristic between ABAQUS and the Component Method (Figure 6.5), it was used the simplification of the moment-rotation characteristic from Eurocode that does not take into account the initial rotational stiffness. An acceptable correlation between the proposed models was obtained, especially during the initial deformation. These results contribute to strengthen the enlargement of the Component Method to 3D; which currently has no validation on standards. On the last step of the simulation, the moment at the joint was 8,5kNm and the last rotation estimated was 35,52mrad. The largest equivalent plastic strain experienced was 2,38% located on the beam flanges at the compression zone. The behavior of the tension and compression zone becomes of great importance to analyze for of these loading conditions. In this case it was taken into account the stresses registered during the analysis. Figures 6.6 and 6.7 show the deformation of the joint on both zones at Von Mises stresses visualization.
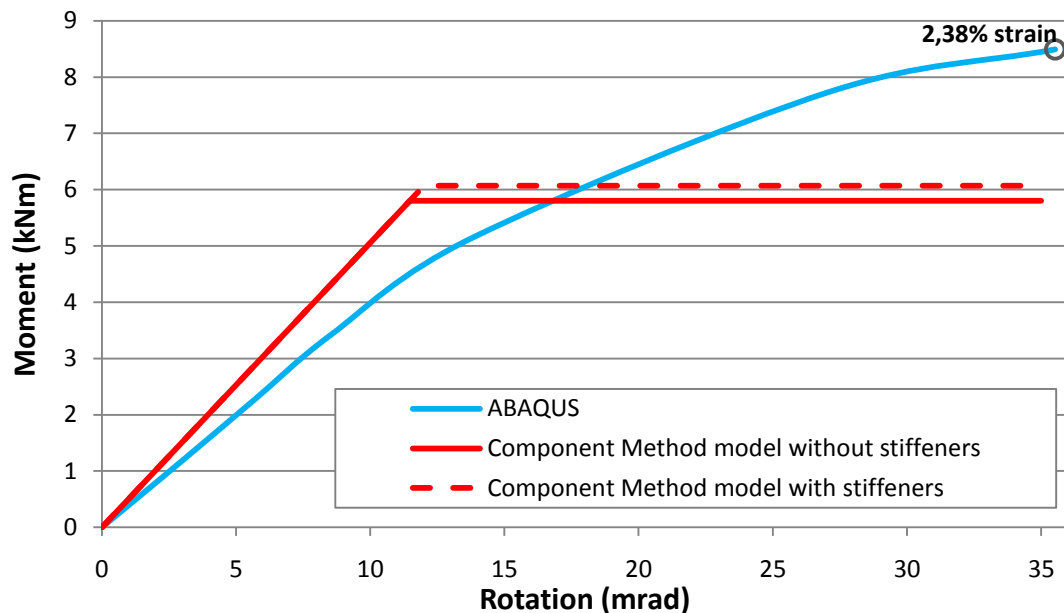
Figure 6.5*: Comparison of moment-rotation between ABAQUS and Component Method model at ambient temperature. Bending moment 8,5kNm around weak axis.*
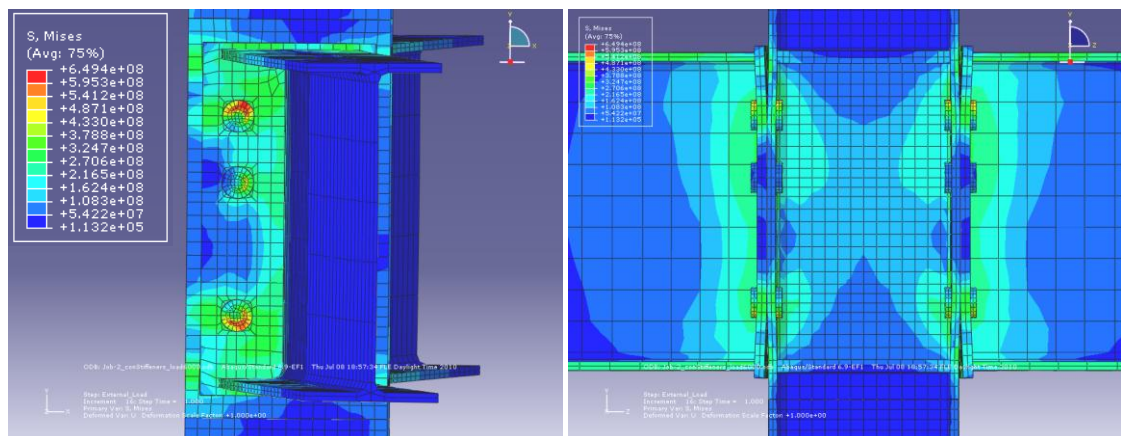
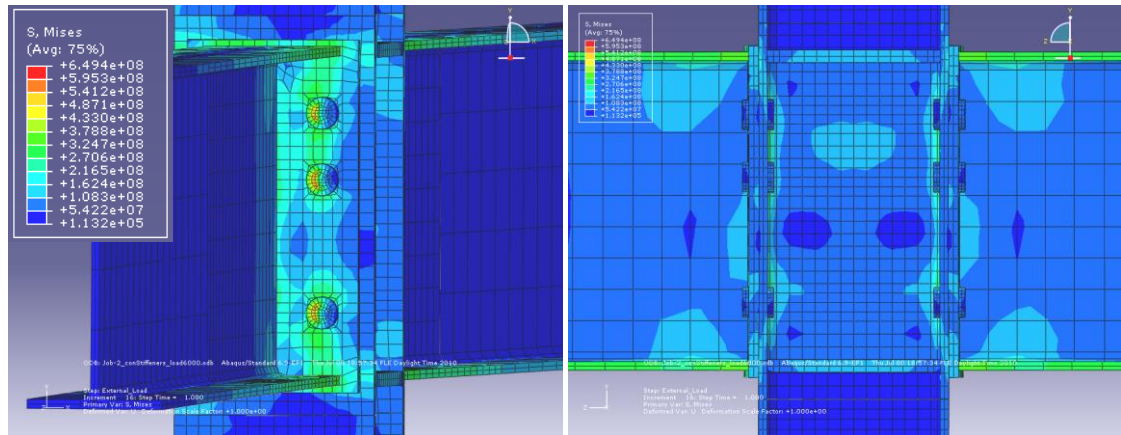***Figure 6.6****: Tension zone (Von Mises stresses in Pa).*

Figure 6.7: *Compression zone (Von Mises stresses in Pa).*

6.3.2. Analysis 2

For the second simulation the loads applied on the beams were 12kN creating a moment at the joint of 17kNm. As a result, the joint experienced a remarkable deformation on the beam flange and endplate as shown on Figure 6.8, and also on the column flanges. The stiffeners at the compression side of the joint suffered some displacement too. The values presented on Figure 6.8 are the displacements on the nodes of the beam flanges at the last step.

For the comparison between FE model and component model on Figure 6.9, the deformation is only represented until 100mrad, but when the analysis was completed the actual last rotation calculated was 332mrad with a 16,98kNm moment. The maximum plastic strain registered was 27,5% at the beam flange. As happened on previous case, the results obtained from ABAQUS show a deformation close to the Component Method, suggesting that the proposed models are capable of predicting the initial stiffness of the joint accurately.

The deformation of the model and stresses on the tension and compression zones are shown on Figures 6.10 and 6.11. The maximum stresses were registered on the bolts of the tension zone (716MPa). A large deformation of the column flange on the tension zone can also be observed. As it was expected, the use of stiffeners has a clearly effect on the joint behavior when deforming. Considering the displacement along the beam flanges representing the joint rotation on both analyses (Figures 6.4 and 6.8); it is highly noticed that the column stiffness does not allow the beam on the compression zone to displace towards the column. When analyzing the plastic strain registered on the simulations, the failure on ABAQUS is found on the column flanges because of convergence. Figure 6.12 shows the model on deformation state and the equivalent plastic strain at the compression zone of one of the flanges when full analysis was accomplished.
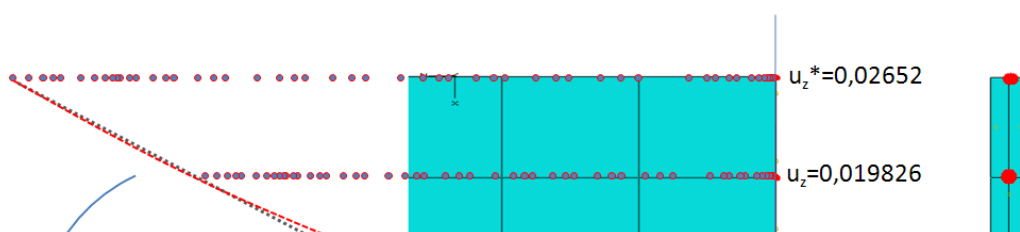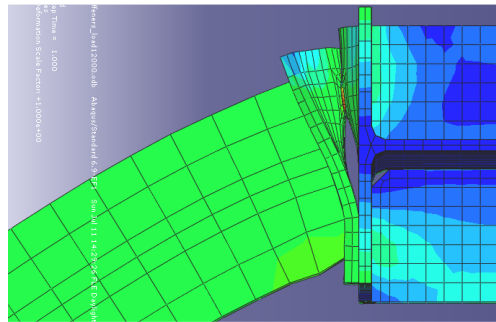
Figure 6.8: *Beam flange displacement with 17kNm bending moment around weak axis (u$_z$ in meters).*
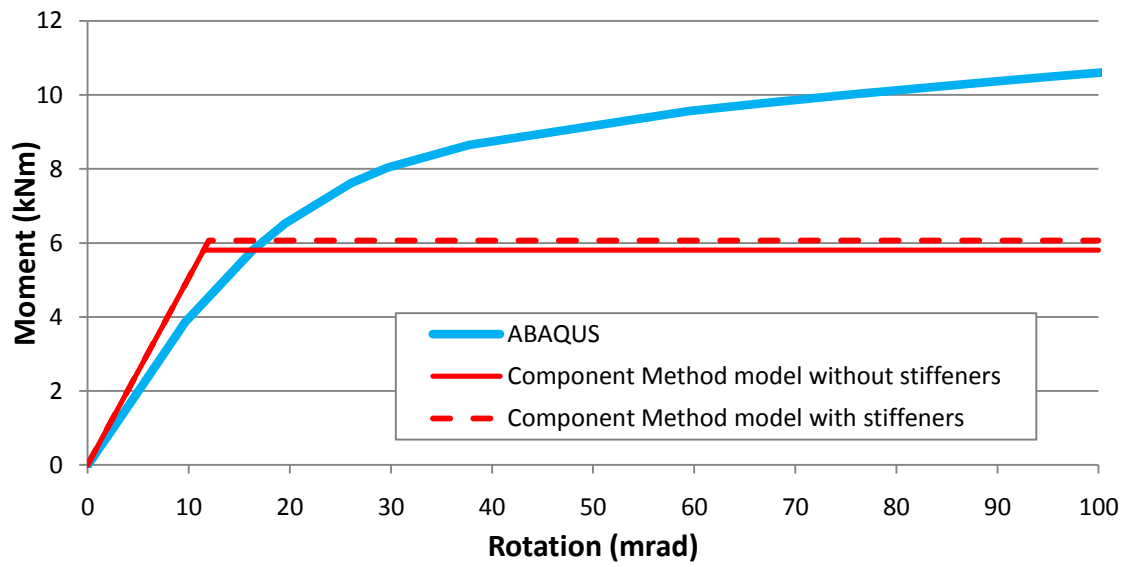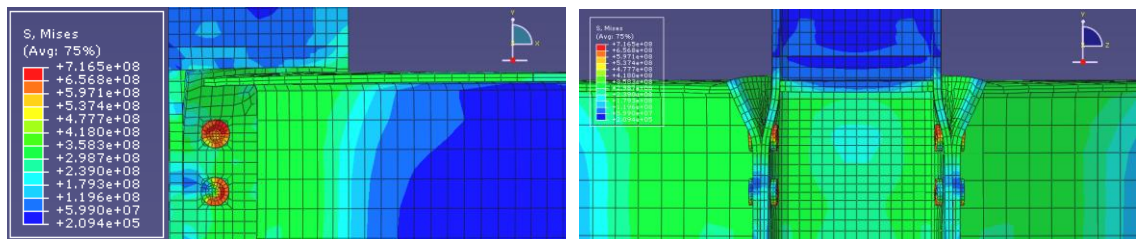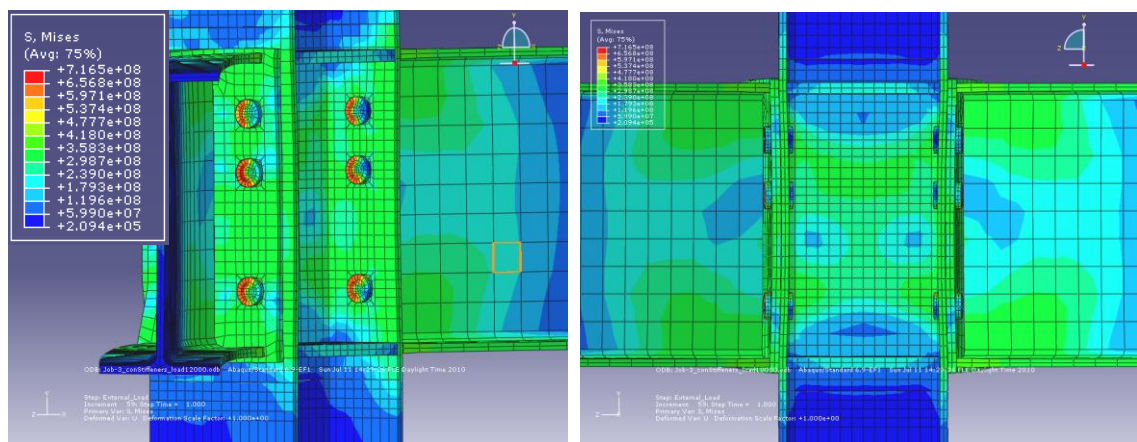

Figure 6.9: *Comparison of moment-rotation between ABAQUS and Component Method model at ambient temperature. Bending moment 17kNm around weak axis.*
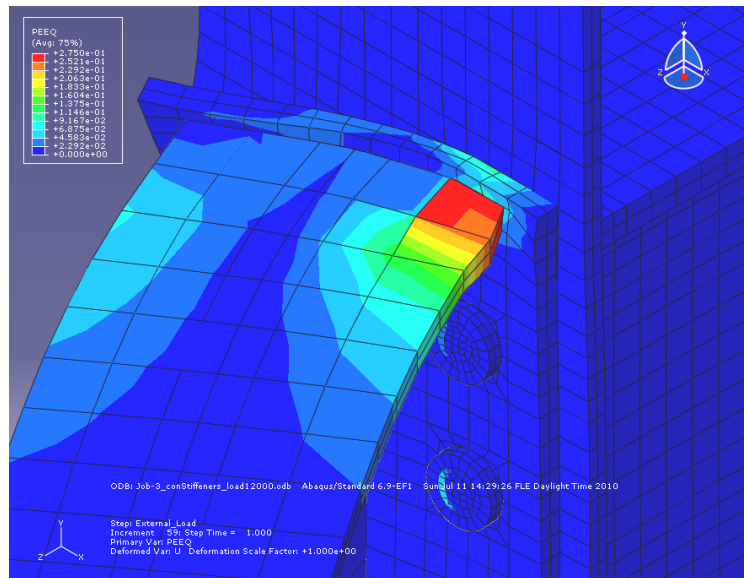
Figure 6.10: Tension zone (Von Mises stresses in Pa). The column flanges experience large deformation due to bending.


*Figure 6.11*: Compression zone (Von Mises stresses in Pa).

Figure 6.12: Failure at the compression zone of beam flange in ABAQUS. Equivalent plastic strain visualization. Moment 17kNm, rotation 326 mrad, and 27,5% maximum plastic strain.

6.3.3. Analysis 3

The last simulation at ambient temperature was performed without stiffeners. The load applied was smaller due to this lost of stiffness on the column. The value of the moment applied at the joint for this case was 2,8kNm. The deformation registered on the beam flange is shown in Figure 6.13. It can be observed that the absence of stiffeners allowed deformation on the column web, and the beam flanges developed displacements on the compression zone. It is also noticed, that this new conditions made possible a symmetric displacement along the flanges, therefore a symmetric rotation. The maximum rotation at the joint after full analysis was estimated at 114mrad with 2,8kNm moment.
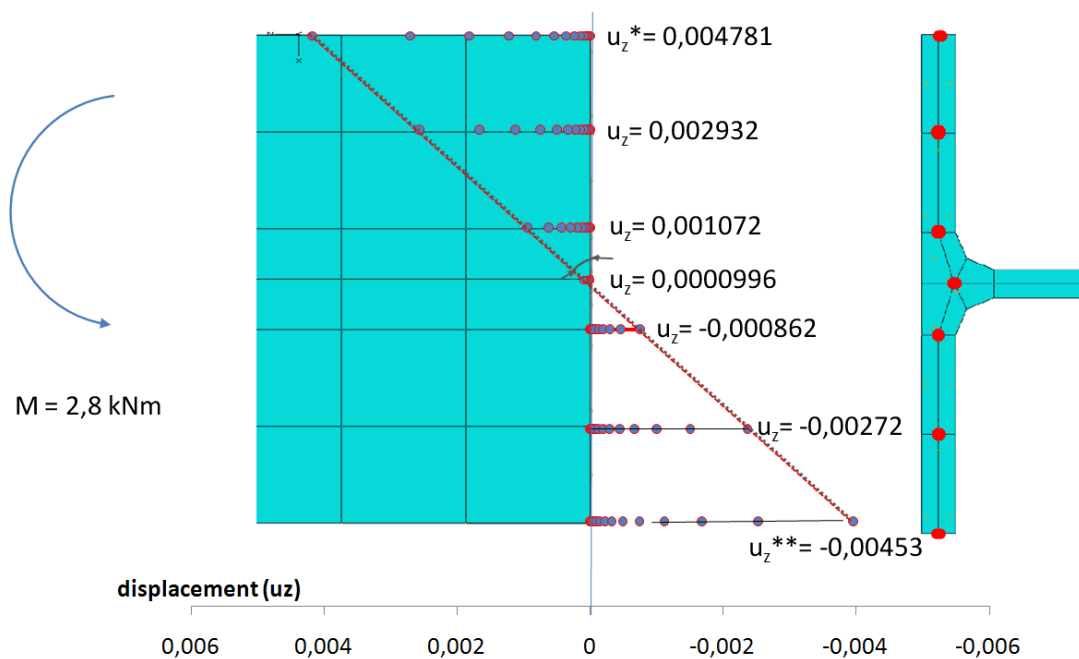

Figure 6.13: Beam flange displacement (values in meters) with bending moment 2,8kNm around weak axis without stiffeners.
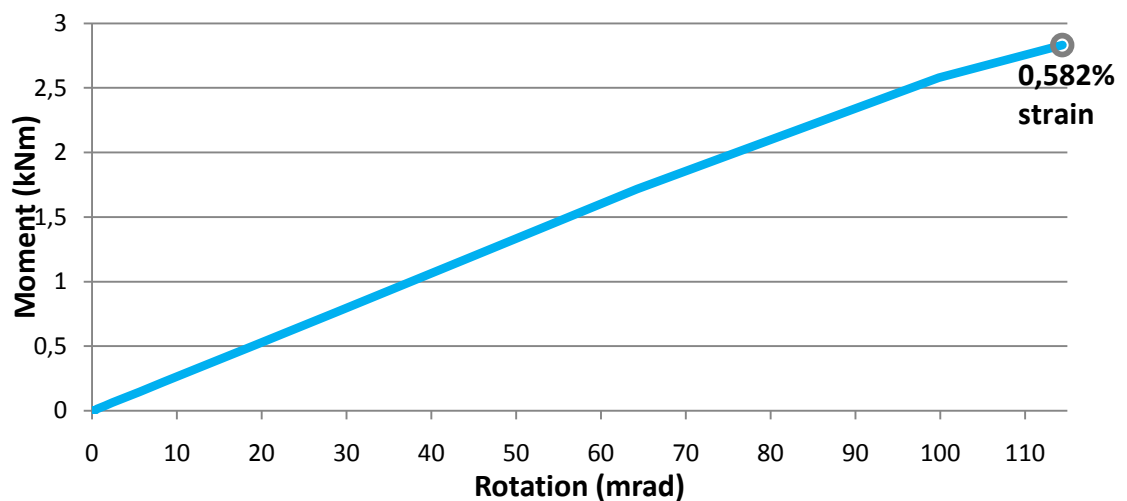

Figure 6.14: Moment-rotation characteristic. Unstiffened column at ambient temperature and 2,8 bending moment around weak axis.

Figure 6.14 shows the moment-rotation characteristic of the simulation. With full analysis, the largest plastic strain at the model (5,82%) was on the column web on the tension side, in line with the bolts as shown on Figure 6.15. The maximum stresses were registered on the tension side of the column web around 300MPa (Figure 6.16). On the compression side there were also large stresses at the column web but only at the level beam flanges.
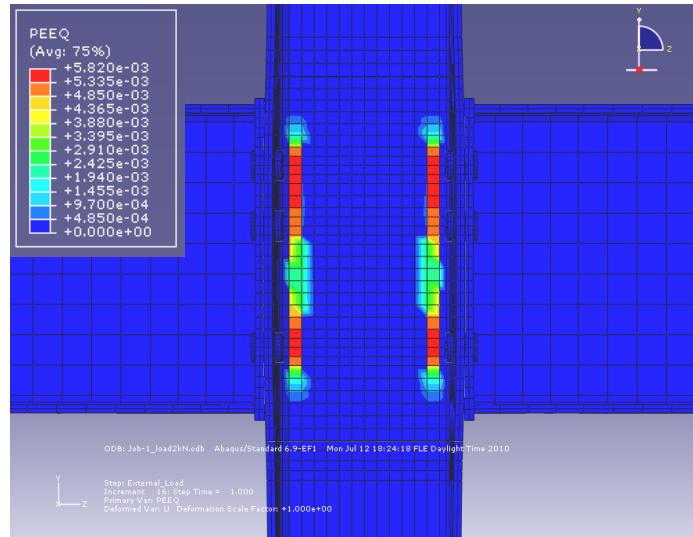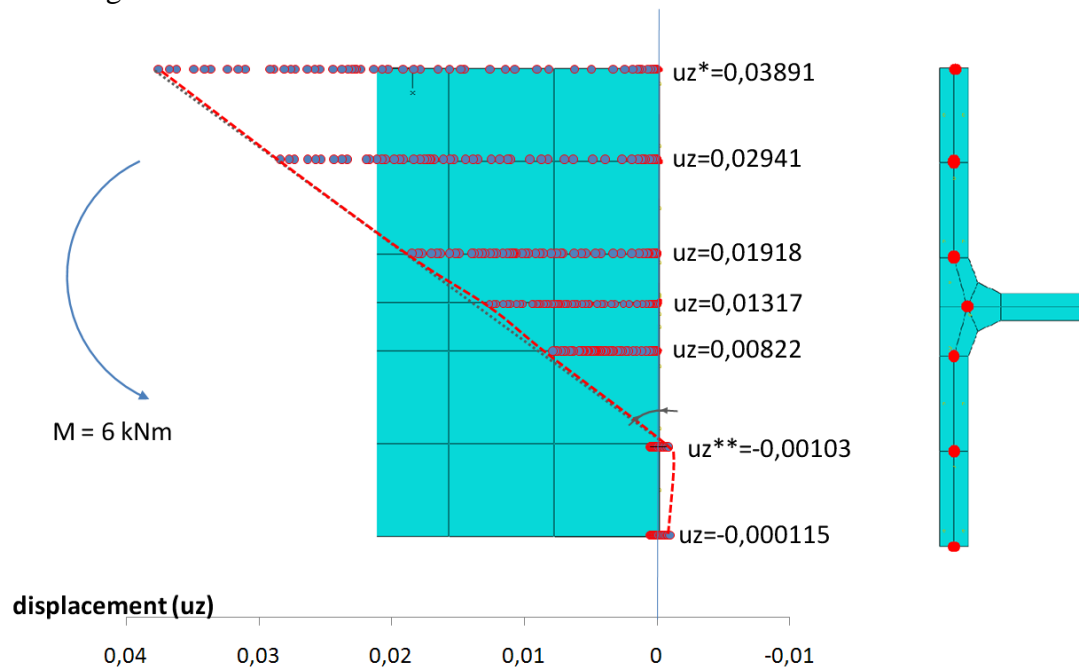

Figure 6.13*: Equivalent plastic strain. Maximum strain value at the tension side of the column web (0,582%).*
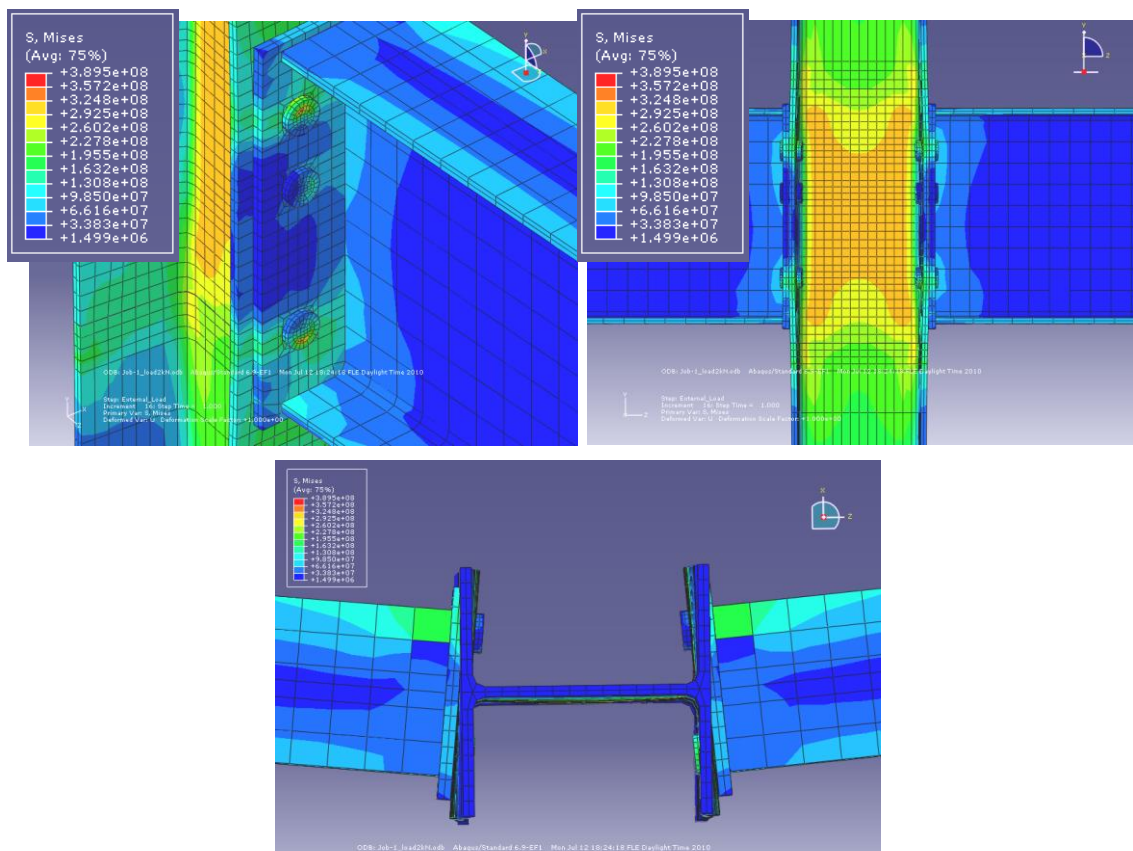

Figure 6.13*: The absence of stiffeners allows deformation on the column web. Maximum stresses at the tension side of the column web.*

6.4.   Results at Elevated Temperatures

The last simulation was carried out at elevated temperatures, using stiffeners at the joint, and applying a 6kNm moment. The values of the displacement at the nodes of the beam flange were as shown on Figure 6.14. Due to steel degradation at elevated temperatures, the rotation experienced was considerably large despite of the small loading. The deformation of the beam flange and endplate can be seen on Figure 6.15. Large distortion was observed, reaching elevated equivalent plastic strains not only on the beam flange and endplate at the compression zone, but also on the bolt shanks and column flange of the tension zone.


Figure 6.14: *Beam flange displacement (values in meters) with bending moment 6kNm around weak axis, stiffeners at the joint and elevated temperatures.*
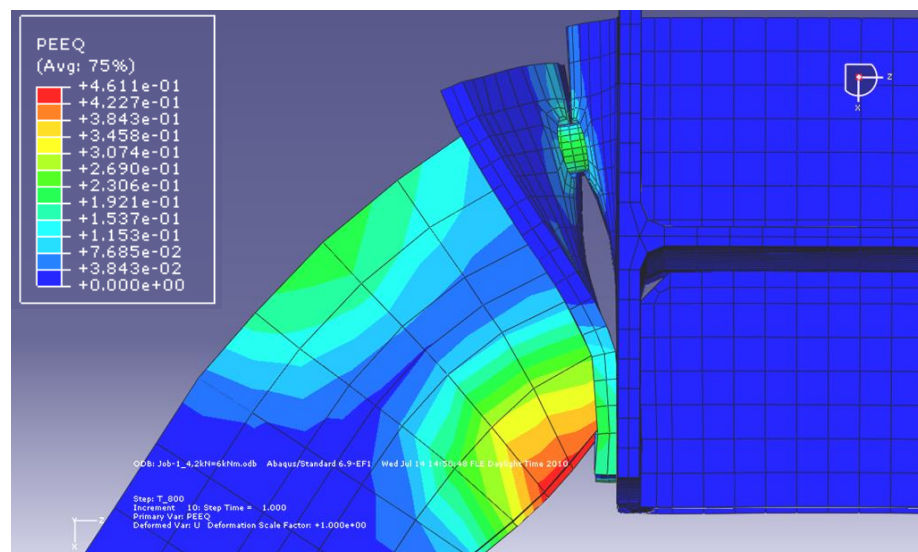

Figure 6.15: *Deformation of the beam and endplate. Equivalent plastic strain visualization. Large distortion at the beam flange, bolts and column flange.*

Structurally speaking, the joint was not designed to resist lateral loading, and with fire conditions this situation is highly noticed on the results. This FE simulation allows some knowledge about the joint resistance with these bending conditions and elevated temperatures. Figure 6.16 shows the joint response with temperature-rotation dependence during the analysis. The information is completed with the plastic strain registered on the beam flange during the process at 500°C, 600°C, 700°C and 800°C. Steel is proposed to fail from 600°C to 700°C, as the 20% plastic strain is reached between these temperatures. Component Method resistance at ambient temperature was 5,8kNm. FEM simulation with 6,0kNm moment shows that the joint can resist this load up to 600-700°C meaning that the Component Method results to be clearly on the safety side.
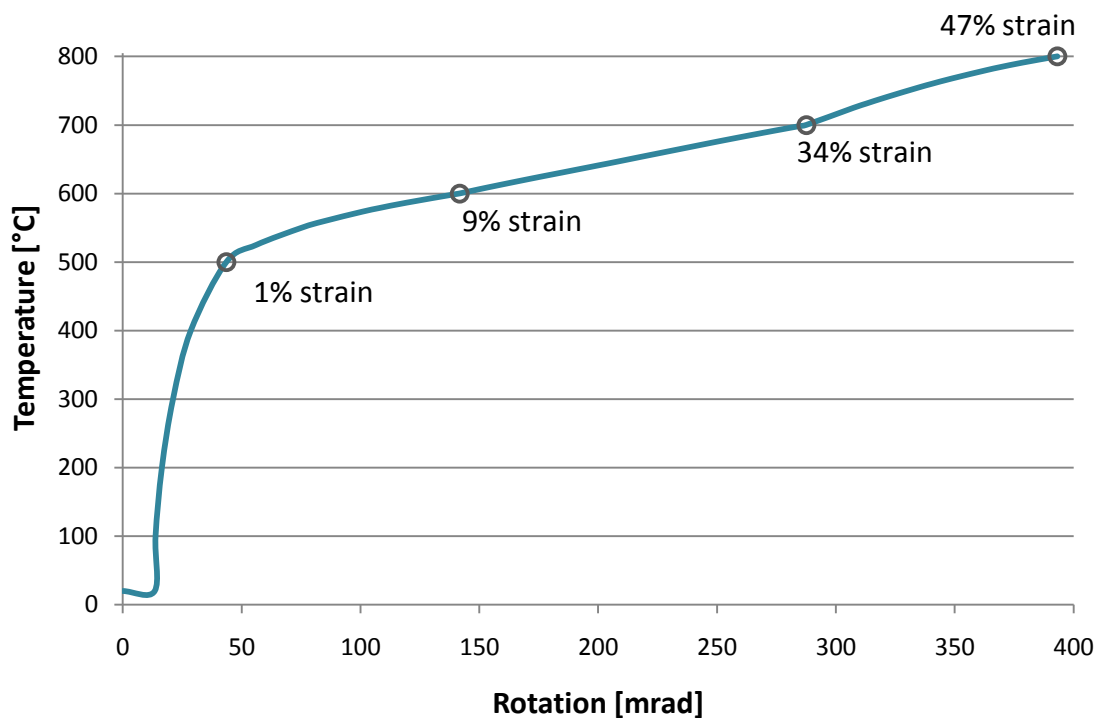

Figure 6.16: *Temperature-rotation characteristic and plastic strain at the beam flange. Maximum rotation was 393mrad at 800°C with 47% plastic strain.*

Figures 6.17 and 6.18 show the tension and compression zones with full analysis accomplished. Apart from the beam flange and endplate, the column flange is observed to experienced large deformation on the tension zone. The stresses registered are also shown on the figures. The maximum values appeared on the beam web at the limit between exposed and no exposed to fire zones.
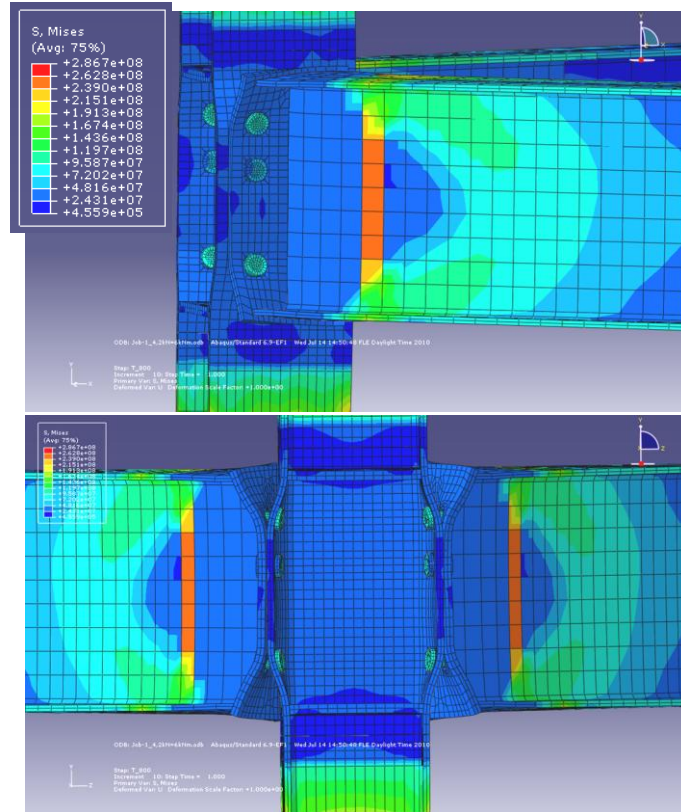
Figure 6.17: Tension zone (Von Mises stresses in Pa) with large deformation on the column flange. Maximum stresses on the beams at the limit with the zone exposed.
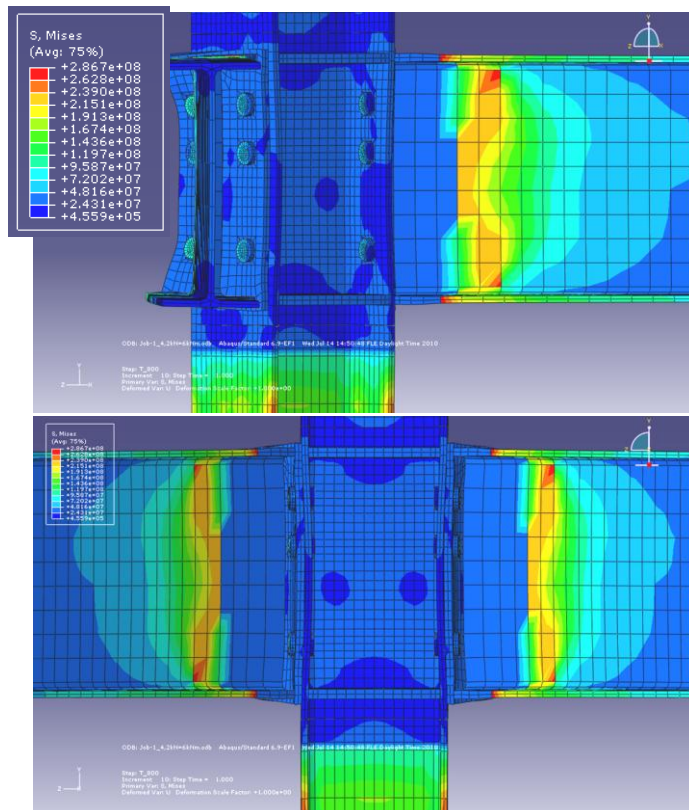
Figure 6.18: Compression zone (Von Mises stresses in Pa).

7.   CONCLUSIONS

The goal of this study was to develop a finite element model able to predict the behavior of an endplate beam-to-column joint at elevated temperatures using ABAQUS solver. Contact elements were crucial for modelling the steel connection performance, and contact interaction between all interfaces was introduced and successfully achieved. The model has been validated against available test results, and after several simulations it was demonstrated to be able to accurately reproduce the experimental conditions. The model incorporates non-linear material properties, but failure could not be performed. Instead, the analysis of plastic strains and large deformations allowed a prediction of the joint failure during the simulations. This proceeding demonstrates close results to experimental tests. Nevertheless, it also involved some difficulties and inaccuracies. In fact, bolt failure was observed to develop bigger distortion at elevated temperatures on FE model than fire tests. This may assume that steel and bolt fracture at elevated temperature, as well as weld performance should have been included in the model to ensure complete faithful prediction of structural behavior.

A Component Method model was also presented to predict the joint response at both ambient and elevated temperatures. The results obtained showed a good agreement with the FE model, which was more noticeable in the elastic zone. Elevated temperatures were introduced applying steel degradation. The main parameters describing stiffness and capacity of the elements were degraded with increasing temperatures by reduction factors. Comparisons with the FE model demonstrate that the use of reduction factors for bolts provide more safety results than reduction factors for yield strength. However, in general the Component Method is capable of predicting the joint behavior at elevated temperatures with a reasonable accuracy especially in the elastic zone.

The finite element model was developed for further study applying 3D loading with bending moment around weak axis. These new conditions gave the chance to enhance the understanding of the joint behavior under fire. Moreover, the Component Method was also extended for these 3D conditions, and comparisons with ABAQUS simulations demonstrate approach between models.

REFERENCES

Airila, M., Ekman, K., Hautala, P. 2003, Design of Machine Parts. WSOY (Finnish).

Al-Jabri, K.S., Burgess, I.W., Plank, R.J. 2005, Spring-stiffness Model for Flexible End-plate Bare-steel Joints in Fire. Journal of Constructional Steel Research. 61, 1672-1691.

Al-Jarbi, K.S. 1999, The Behaviour of Steel and Composite Beam-to-column Joints in fire. Ph.D. Thesis. Department of Civil and Structural Engineering, University of Sheffield, UK.

Dassault Systèmes Simulia Corp. 2009, Getting Started with ABAQUS/CAE: Interactive Edition.

EN 1993-1-1. 2005. Eurocode 3: Design of Steel Structures. Part 1-1: General Rules and Rules for Buildings. CEN, Brussels, Belgium.

EN 1993-1-2, 2005. Eurocode 3: Design of Steel Structures. Part 1-2: General Rules. Structural Fire Design. CEN, Brussels, Belgium.

EN 1993-1-8, 2005. Eurocode 3: Design of Steel Structures. Part 1-8: Design of Joints. CEN, Brussels, Belgium.

Heinisuo, M., Laine, V., Lehtimäki E. 2009. Enlargement of the component method to 3D. Proceedings of Nordic steel conference, September 2-4, Malmö, Sweden. pp. 400-436.

Hibbitt, Karlsson and Sorsen, Inc. 2001, ABAQUS/Standard User's Manual. Volume II.

Hu, Y., Davison, B., Burgess, I., Plank, R. 2009, Component Modelling of Flexible End-plate Joints in Fire. Steel Structures. 9, 1-15.

Sarraj, M. 2007, The Behaviour of Steel Fin-plate Joints in Fire. PhD Thesis. University of Sheffield, UK.

Sarraj, M., Burgess, I.W., Davison, J.B, Plank, R.J. 2007, Finite element modeling of steel fin plate joints in fire. Fire Safety Journal. 42, 408-415.

Theodorou, Y. September 2001,Mechanical properties of grade 8.8 bolts at elevated temperatures. Master of Science Thesis. Department of Civil and Structural Engineering, University of Sheffield, UK.

Wang, W.Y., Li, G.Q., Dong, Y.L. 2007, Experimental study and spring-components modelling of extended end-plate joints in fire. Journal of Constructional Steel Research. 63, 1127-1137.

Yu, H., Burgess, I.W., Davison, J.B., Plank, R.J. 2008, Numerical simulation of bolted steel joints in fire using explicit dynamic analysis. Journal of Constructional Steel Research. 64, 515-525.